MCB
Journals.ASM.org

Molecular Characterization of Prospectively Isolated Multipotent Mesenchymal Progenitors Provides New Insight into the Cellular Identity of Mesenchymal Stem Cells in Mouse Bone Marrow

Hong Qian,[a,b] Aurora Badaloni,[c] Francesca Chiara,[c] Jenny Stjernberg,[a] Naresh Polisetti,[a] Kristian Nihlberg,[a] G. Giacomo Consalez,[c] Mikael Sigvardsson[a]

Department of Clinical and Experimental Medicine, Faculty of Health Sciences, Linköping University, Linköping, Sweden[a]; Center for Hematology and Regenerative Medicine, Department of Medicine, Karolinska Institute Huddinge, Stockholm, Sweden[b]; Division of Neuroscience, San Raffaele Scientific Institute, Milan, Italy[c]

Despite great progress in the identification of mesenchymal stem cells (MSCs) from bone marrow (BM), our knowledge of their *in vivo* cellular identity remains limited. We report here that cells expressing the transcription factor *Ebf2* in adult BM display characteristics of MSCs. The *Ebf2*$^+$ cells are highly clonal and physiologically quiescent. *In vivo* lineage-tracing experiments, single cell clone transplantations, and *in vitro* differentiation assays revealed their self-renewal and multilineage differentiation capacity. Gene expression analysis of the freshly sorted *Ebf2*$^+$ cells demonstrated the expression of genes previously reported to be associated with MSCs and the coexpression of multiple lineage-associated genes at the single-cell level. Thus, *Ebf2* expression is not restricted to committed osteoblast progenitor cells but rather marks a multipotent mesenchymal progenitor cell population in adult mouse BM. These cells do not appear to completely overlap the previously reported MSC populations. These findings provide new insights into the *in vivo* cellular identity and molecular properties of BM mesenchymal stem and progenitor cells.

Bone marrow (BM) contains a heterogeneous population of stromal cells involved both in the regulation of hematopoiesis and in the maintenance of the BM microenvironment (1–4). This stromal cellular compartment contains osteoblasts, adipocytes, endothelial cells, immature stromal progenitor cells, and a rare population of multipotent progenitors, including mesenchymal stem cells (MSCs). MSCs were originally identified in BM by their capacity to form CFU-fibroblasts (CFU-Fs) *in vitro* (5). These cells have the potential to differentiate into multiple mesenchymal cell lineages such as osteoblasts, adipocytes, and chondrocytes *in vitro* (6, 7). It has been assumed that the stromal cells in BM are hierarchically organized with MSCs at the apex, followed by more differentiated cells with reduced expansion capacity and limited lineage potential (8, 9). Much of our current understanding of the mesenchymal stem and progenitors has been extracted from *in vitro* studies that, even although informative, still may not provide reliable information about the true identity and properties of the MSCs. Recent developments in flow cytometry-based methods has allowed for the direct isolation of MSCs from BM. It has been shown that MSCs from mouse BM express *Nestin*, platelet-derived growth factor receptor α (PDGFRα), and stem cell antigen 1 (SCA1) (10–13) but not CD44 (14). These findings have opened new possibilities to help us better understand the biological properties of MSCs in mouse BM. However, these defined MSC populations remain very heterogenous.

Early B-cell factor 2 (Ebf2) is a transcription factor expressed in immature osteoblastic cells (15, 16), adipocytes (17, 18), neurons (19, 20), and stromal cell lines (21). In the BM, the protein has been suggested to be important for osteoblast-dependent differentiation of osteoclasts during fetal development and for formation of the hematopoiesis-supporting microenvironment (15, 16). We here report that *Ebf2* expression is not limited to lineage-restricted progenitors but rather defines an MSC population. *In vivo* lineage tracing of the *Ebf2*$^+$ cells demonstrated their physiological contribution to generation of both osteoblasts and chondrocytes. These cells are highly enriched with CFU-Fs and phenotypically resemble MSCs. Importantly, our *in vitro* assays, *in vivo* transplantations, and molecular analyses of single *Ebf2*$^+$ cell clones revealed their multilineage differentiation potential and self-renewal capacity. These findings provide new evidence for cellular identity of the *Ebf2*$^+$ cells and novel insights into the molecular features of MSCs in adult mouse BM.

MATERIALS AND METHODS

Mice. Nine- to fifteen-week-old Tg(*Ebf2*-GFP) FVB/N transgenic (Tg) mice were provided by the Mutant Mouse Regional Resource Center (USA) (22). Tg(*Ebf2*-CreER^{T2}) mice were generated as described below. Tg(*Ebf2*-CreER^{T2}) mice were crossed with Gt(Rosa)26Sor$^{tm1(EYFP)Cos}$ mice having a loxP-flanked transcriptional stop sequence preceding the *eYFP* gene, under the control of the ubiquitous *Rosa26* promoter (Jackson Laboratories) (Fig. 1A). Eight-week-old bitransgenic (*Ebf2*-CreER^{T2})/Gt(Rosa)26Sor$^{tm1(EYFP)Cos}$ mice were injected intraperitoneally with 4 mg of tamoxifen (Sigma catalog no. T5648) dissolved in corn oil for five consecutive days. Animal procedures were performed with approval from the local ethics committee at Linköping University (Linköping, Sweden).

Generation of Tg(Ebf2-CreER^{T2}) mice. For the generation of Tg(*Ebf2*-CreER^{T2}) mice, the RP24-283N8 bacterial artificial chromosome (BAC) clone, consisting of 32 kb of 5′-flanking sequence plus the first

Received 20 September 2012 Returned for modification 22 October 2012
Accepted 19 November 2012
Published ahead of print 26 November 2012
Address correspondence to Hong Qian, hong.qian@ki.se.
Supplemental material for this article may be found at http://dx.doi.org/10.1128/MCB.01287-12.

doi:10.1128/MCB.01287-12

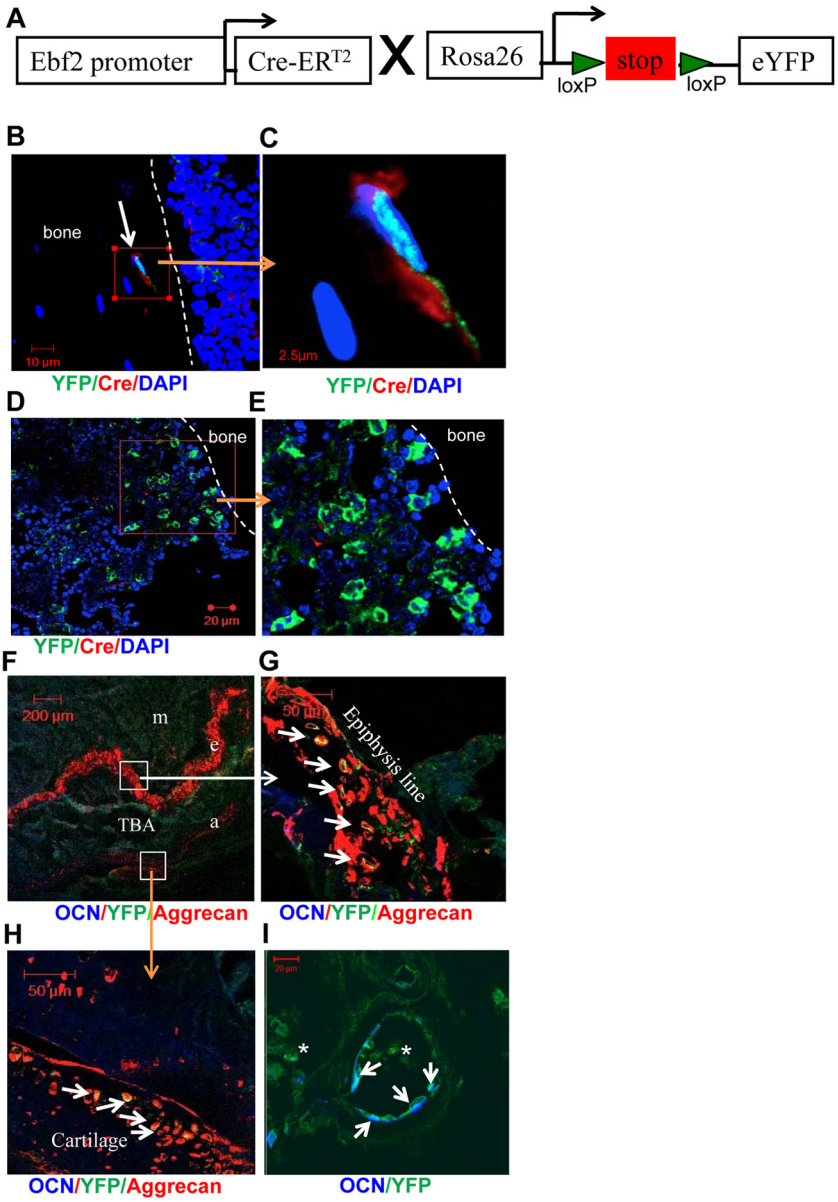

FIG 1 Lineage-tracing experiments suggest the physiological contribution of *Ebf2*$^+$ cells to the generation of osteoblasts and chondrocytes. Bitransgenic [Tg(*Ebf2*-CreER^{T2} × Rosa26-*Yfp*)] mice were utilized. (A) Scheme of constructs used for lineage-tracing experiments. The construct for generation of Tg(*Ebf2*-CreER^{T2}) mice was produced by BAC recombineering. A BAC clone consisting of 32 kb of 5′-flanking sequence plus the first seven exons of the murine *Ebf2* gene (BACPAC Resource Center, Oakland, CA) was recombineered in *E. coli* to insert tamoxifen-inducible CreER^{T2} and selectable markers in the first coding exon to replace the endogenous ATG of Ebf2. This mouse strain was generated and crossed with mice having a loxP-flanked transcriptional stop sequence preceding the *eYFP* gene, under the control of the ubiquitous *Rosa26* promoter (Jackson Laboratories). (B to I) *In situ* analysis of *Ebf2*$^+$ cell-derived progeny. The femoral sections were from the bitransgenic mice 11 weeks (B to E) and 32 weeks (F to I) after tamoxifen treatment. (B and C) Single *Ebf2*$^+$ cell (Cre$^+$ YFP$^+$) in the bone surface (dashed line). The cells were stained with DAPI (blue), anti-GFP (green), and anti-Cre (red). (C) Enlarged image of the Cre$^+$ YFP$^+$ cells in the gated region. (D and E) A YFP$^+$ cell cluster in the endosteal region. (E) Enlarged image of the cluster. (F to H) *Ebf2*$^+$ cell-derived chondrocytes (aggrecan$^+$ YFP$^+$) at the epiphysis line (e) and articular cartilage (a). m, marrow; TBA, trabecular area. (I) *Ebf2*$^+$ cell-derived osteoblasts (OCN$^+$ YFP$^+$).

seven exons of the murine *Ebf2* gene, was obtained from the BACPAC Resource Center at Children's Hospital Oakland Research Institute, Oakland, CA. By BAC recombineering (23, 24), the genomic clone was modified to insert a cDNA encoding the tamoxifen-inducible CreER^{T2}, followed by the simian virus 40 polyadenylation signal in the first coding exon of the *Ebf2* gene. The BAC DNA was microinjected into the pronucleus of FVB/N oocytes. Pups were analyzed by Southern blotting for the presence of the transgene. Founders were isolated and a transgenic line was established mating the founders with FVB/N mice. The primers used for the genotyping of *Ebf2/CreER* were *Cre-ER*-Forward (5′-CCGGAGA TCATGCAAGCTG-3′) and *Cre-ER*-Reverse (5′-CATGTGAACCAGCT CCCTG-3′). The product is 350 bp. PCR amplification conditions were as follows: 95°C for 2 min, 95°C for 30 s, and 60°C for 30 s for 30 cycles, followed by 72°C for 30 s and then 72°C for 5 min.

Isolation of mononuclear cells from mouse BM. Mononuclear cells were isolated from mouse BM as described previously (14). Briefly, femurs, tibias, and iliac crest were crushed in phosphate-buffered saline (PBS) plus 10% fetal bovine serum (FBS; PAA Laboratories). The marrow

cells were collected. The cells from bone were obtained by treatment of bone fragments with 0.1% collagenase II (CLS II Worthington Biochemicals) and 0.05% trypsin-EDTA for 30 to 45 min at 37°C. The bone and marrow cells were pooled and spun down at 300 × *g* for 5 to 10 min and then resuspended in PBS plus 10% FBS for MSC isolation.

Multicolor fluorescence-activated cell sorting (FACS) isolation and analysis of MSCs. The hematopoietic cells in the BM mononuclear cell preparations were first depleted by staining the cells with purified rat anti-mouse CD45 and the hematopoietic lineage (LIN) markers TER119, B220, CD4, CD8, GR1, and MAC1 and subsequently using sheep anti-rat Dynal beads (Invitrogen) as described previously (25). The remaining hematopoietic cells were visualized by using goat anti-rat tricolor antibody and fluorescence-conjugated CD45, TER119, and CD19 for the further removal of hematopoietic cells. Dead cells were excluded by propidium iodine (PI) staining. The *Ebf2*$^+$ and *Ebf2*$^-$ stromal cells were sorted or analyzed based on green fluorescent protein (GFP) expression on a FACS Aria II Sorp (BD). GFP$^+$ cells were gated according to the fluorescence minus one (FMO) method using cells from nontransgenic mice. See Table S1 in the supplemental material for detailed information about the antibodies used here.

Microarray analysis. RNA from sorted *Ebf2*$^+$ and *Ebf2*$^-$ cells was extracted as previously described (14), labeled, and amplified according to the Affymetrix GeneChip expression analysis technical manual. Chips are scanned using GeneChip Scanner 3000. Mouse Genome 430.2.0 chips were normalized using invariant set normalization, and probe level expression values were calculated using the PM-MM model provided by the dCHIP software (www.dchip.org).

CFU-F assay. CFU-F assay of BM stromal cells (CD45$^-$ LIN$^-$ *Ebf2*$^{+/-}$) was performed as described previously (14). The cells were cultured in the complete MesenCult medium (catalog no. 5511; Stem Cell Technologies) under normoxic (20% O_2) or hypoxic (1% O_2) conditions for 9 to 10 days.

Expansion and self-renewal assay of MSCs. CD45$^-$ LIN$^-$ *Ebf2*$^+$ and *Ebf2*$^-$ cells were seeded in 12-well plates containing medium from MesenCult proliferation kit (catalog no. 5511; Stem Cell Technologies) for the expansion of MSCs. The assay was performed under hypoxic conditions (1% O_2; Innova CO-14 incubator; New Brunswick Scientific Co., Edison, NJ). After 7 to 8 days of culture, the cells were trypsinized with 0.05% trypsin-EDTA (Gibco) and collected for counting and resorting or analysis of GFP/*Ebf2* expression. The *Ebf2*$^+$ and *Ebf2*$^-$ cells from primary or the cultured *Ebf2*$^+$ cells at earlier passage were sorted and replated in a new 12-well plate for further sorting or analysis. The fold expansion of the test cells was calculated based on the input cell numbers, the total cell counts, and the frequency of the cell subsets (GFP$^{+/-}$ cells) at different passages.

***In vitro* differentiation assay.** This protocol was modified from the previously described (12) for evaluation of multiple differentiation potential of a single cell-derived colony. The cells in one CFU-F derived from single CD45$^-$ TER119$^-$ Ebf2$^+$ cells were split into three conditions with differentiation induction media for osteoblast, adipocyte, and chondrocytes differentiation. The media were changed twice a week for 21 to 28 days. For osteoblast differentiation, the cells were cultured in complete α minimum essential medium or Dulbecco modified Eagle medium (DMEM) containing 10% FBS, 10 mM HEPES (1 M), 100 U of penicillin/ml, 100 μg of streptomycin/ml, 50 μg of ascorbic acid (Sigma)/ml, 1 × 10^{-7} to 5 × 10^{-7} M dexamethasone (Sigma), and 10 mM glycerol phosphate or complete osteogenic medium mixed by human/mouse StemXVivo osteogenic/adipogenic base medium (CCM007) and mouse StemXVivo osteogenic supplement (CCM009; R&D Systems). At days 21 to 28 after induction, the cells were fixed with 10% formalin or ice-cold methanol and stained with 1% alizarin red S (Sigma) (pH 4.1) for 5 to 10 min. The excess dye was then removed, and the wells were dehydrated and subsequently mounted using Clear-Mount mounting solution (Invitrogen, CA). For adipogenesis, the cultures were incubated in DMEM GlutaMax (Gibco) supplemented with 10% FBS, 10 mM HEPES,100 U of penicillin/ml, 100 μg of streptomycin/ml, 5 to 10 μg of insulin (Sigma)/ml, 20 μM indomethacin (Sigma), or 0.5 mM isobutylmethylxanthine (Sigma), 1 × 10^{-7} to 5 × 10^{-7} M dexamethasone (Sigma) or in the complete adipogenic media mixed by 1 part of adipocyte stimulatory supplement (catalog no. 05503) and 4 parts of MesenCult MSC basal medium (catalog no. 05501; Stem Cell Technologies). The cells were fixed with 10% formalin and stained with 0.5% oil red O (Sigma) in methanol (Sigma). The chondrocyte differentiation was induced in monolayer culture, and the cells were cultured in 96- or 12-well plates in complete DMEM plus high glucose at 4.5 g/liter containing 10^{-7} M dexamethasone, 1% ITS (a mixture of recombinant human insulin, human transferrin, and sodium selenite; Sigma), 2 mM sodium pyruvate (Sigma), 0.35 mM proline (Sigma), and 10 ng of TGF-β3 (R&D Systems)/ml or complete chondrocyte differentiation medium (mixed with StemXVivo human/mouse chondrogenic supplement [catalog no. CCM006] and StemXVivo human/mouse chondrogenic base medium [catalog no. CCM005] at a 1/100 ratio [R&D Systems]). The chondrocyte differentiation was verified by staining of proteoglycan with both toluidine blue (Sigma; pH 2.0 to 2.5) and 1% Alcian blue in 3% acetic acid solution (pH 2.5). We then removed the excess dye and washed the samples three times with distilled water. The plates were then mounted with Clear-Mount mounting solution. The images were taken using a bright field.

Multiplex single-cell RT-PCR analysis. Multiplex single-cell reverse transcription-PCR (RT-PCR) analysis was performed as previously described (26, 27). The genes analyzed included the chondrocyte genes *Pref1*, *Sox9*, and *Col2a1*, the osteoblast genes *Opn*, *Col1a1*, and *Runx2/Osf2*, and the adipocyte genes *Pparg*, *ApoD*, and *Pref1*. *Pref1* was considered the master gene for both chondrocyte and adipocyte differentiation (28). For the sequences of nested PCR primers, see Table S2 in the supplemental material.

Quantitative RT-PCR. The cells were sorted directly into buffer-RLT and frozen at −80°C. RNA extraction and DNase treatment was performed with a RNeasy Micro kit (Qiagen) according to the manufacturer's instructions for samples containing $<10^5$ cells. Eluted RNA samples were reverse transcribed using SuperScript III and random primers (Invitrogen) according to the protocol supplied by the manufacturer. Real-time quantitative PCRs were performed by mixing 2× TaqMan universal PCR master mix, 20× TaqMan primer-probe mix, RNase-free H_2O, and 5 μl of cDNA for a final reaction volume of 20 μl. For information about Assays-on-Demand probes, see Table S3 in the supplemental material.

Immunohistochemistry staining. The mice were perfused through heart by PBS or 0.9% normal saline, followed by fixative Stefanini solution (2% paraformaldehyde plus 0.03% picric acid in PBS [pH 7.4]) after cervical dislocation. Femurs and tibias were removed and fixed for 2 days in Stefanini solution at 4°C and decalcified in 10% EDTA (pH 7.2) for 5 to 7 days. Thereafter, they were placed in 20% sucrose-PBS overnight and embedded in frozen-specimen embedding medium (OCT compound; Tissue-Tek, Netherlands) at −80°C. Bones were cryosectioned in 5- to 10-μm sections using a Cryostat CM3050 (Leica, Germany). The sections were incubated with Background Eraser (Biocare Medical) for at least 30 min at room temperature prior to the staining of specific antibodies. The immunohistochemistry staining was performed as described previously (29). The GFP or yellow fluorescent protein (YFP) expression was visualized by primary chicken anti-GFP antibody (Abcam), which can recognize both GFP and YFP, and was followed by the secondary rabbit or donkey anti-chicken IgY–fluorescein isothiocyanate (FITC; Abcam or Jackson Immunoresearch Laboratories). The collagen type II and aggrecan were visualized by first rabbit polyclonal anti-collagen type II (Abbiotec, LLC, San Diego, CA) and rabbit antiaggrecan (Millipore) and the secondary donkey anti-rabbit antibody conjugated to Alexa Fluor 647 (Invitrogen) or Cy5 (Jackson Immunoresearch). Goat anti-mouse osteocalcin (ABD Serotec and Acris Antibodies GmbH) and Alexa Fluor 350–donkey anti-goat IgG (H+L; Invitrogen) were used for the staining of osteocalcin. Rabbit anti-Sp7/Osterix antibody (ab22552; Abcam) and donkey anti-rabbit antibody–Alexa Fluor 488 were used for detecting os-

terix$^+$ cells in the transplanted ceraforms. The endothelial cells were stained with rabbit anti-mouse CD31 polyclonal antibody (ab28364) or rat anti-mouse antibody CD31 (MEC13.3; Biolegend), followed by donkey anti-rabbit antibody–Alexa Fluor 647 (Invitrogen) or goat anti-rat IgG (Fab)2 TRITC (Santa Cruz). Nestin expression was detected by anti-mouse monoclonal antibody (Abcam catalog no. ab6142) and donkey F(ab′)2 polyclonal secondary antibody to mouse IgG(H&L) (DyLight 650, catalog no. ab98769; Abcam), and SCA1 was determined by rat anti-Sca1 antibody D7-biotin monoclonal antibody (Abcam catalog no. ab25196) and steptavidin-Cy5 (Invitrogen). The sections were mounted with Vectashield mounting medium with or without DAPI (4′,6′-diamidino-2-phenylindole; Vector Laboratories) and covered with coverslips before inspection. The images were taken using Zeiss META 510 confocal microscope.

Heterotopic transplantation of the *Ebf2*$^+$ cells. The *Ebf2*$^+$ cells expanded from single *Ebf2*$^+$ clones were transduced with retrovirus mStrawberry vector at passages 9 to 11. The virus supernatant was produced as described previously (30). The expanded *Ebf2*$^+$ cells were incubated with the virus supernatant for 3 days in a 6-well plate precoated with retronectin (TaKaRa catalog no. T100B; 25 μg/ml) in the presence of Polybrene (0.5 μg/ml). The infected cells were sorted for the expression of mStrawberry by using the BD FACS Aria Sorp system. The sorted mStrawberry$^+$ cells were then cultured in DMEM plus 10% FBS for 2 to 3 weeks in order to get a sufficient number of the cells for transplantation. ceramic cubes (ceraforms [3 by 3 by 3 mm]; Teknimed, France) were washed with bidistilled water twice and coated with 0.1 mg of fibronectin/ml from bovine plasma (Sigma). The coating procedure under negative pressure was performed as described previously (10). The ceraforms were dried in a sterile hood for 24 h. Then, 4.5×10^5 mStrawberry$^+$ *Ebf2*$^+$ cells were loaded into the ceraforms for 24 h in a normoxic incubator. The ceraforms were implanted subcutaneously under dorsal skin of anesthetized adult FVB/N mice. The mice were treated with antibiotics for 2 weeks after implantation.

FACS and histology analysis of ossicles. The ceraforms from the recipient mice were harvested into PBS plus 5% FBS for FACS or for histology analysis at 6 to 7 weeks after transplantation. For FACS analysis, the ceraforms were washed with PBS twice before incubation with 0.05% trypsin-EDTA (Gibco) and 0.1% collagenase type II (CLS II; Worthington Biochemicals) for 45 min at 37°C on a shaker at the speed of 300 rpm/min. The detached cells were collected and subjected to the staining of CD45, TER119, and CD31 to sort donor cells and derived mesenchymal cells (mStrawberry$^+$ CD45$^-$ TER119$^-$ CD31$^-$). The cells obtained from no-donor-cell-loaded ceraforms were used as the FMO control for setting a gate of mStrawberry$^+$ stromal cells, and an *in vitro* mixture of these cells with culture-expanded mStrawberry$^+$ *Ebf2*$^+$ cells was used as a positive control for mStrawberry and for making other FMO controls. For histology analysis, the ceraforms underwent decalcification for 10 to 14 days in 10% EDTA (pH 7.2) after fixation and were cryoprotected and sectioned (7 μm) using a Cryostat Leica CM3050 apparatus (Leica, Germany). The sections were stained with hematoxylin and eosin Y (H&E) as described previously (31). Osteocalcin and osterix expression were detected by goat antiosteocalcin (BP712; Acris Antibodies GmbH), followed by donkey anti-goat antibody–Alexa Fluor 350 (Invitrogen) and rabbit antiosterix (Abcam) polyclonal antibody, followed by donkey anti-rabbit antibody–Alexa Fluor 647 (Invitrogen). Fluorescent images were taken using a Zeiss META 510 confocal microscope, and H&E images were taken using Leica Application Suite software.

Cell cycle analysis. BM cells were initially stained with antibodies against CD45 and lineages mentioned above. The cells were then fixed and stained with phycoerythrin-conjugated anti-KI-67 antibody using a Cytofix/Cytoperm kit (BD Biosciences) and DAPI, as described previously (14). The BM cells from nontransgenic mouse were fixed after cell surface staining; FMO for GFP gating and the live cells from the transgenic *Ebf2-Egfp* mice without fixation were used as controls for any fixation-related changes of fluorescent signals. Analysis was performed on a FACS Aria II SORP (BD).

Statistical analysis. An unpaired or paired *t* test was used to compare the differences between different cell populations. All reported *P* values were obtained using GraphPad Prism 4.0 software, and a *P* value of <0.05 was considered statistically significant. The frequencies of CFU-Fs were calculated by L-Calc software (Stem Cell Technologies, Inc.).

RESULTS

***Ebf2*$^+$ cells contribute to the generation of osteoblasts and chondrocytes *in vivo*.** It has been proposed that *Ebf2* expression is restricted to a small population of osteoblast progenitors in the fetal bone (15); however, the downregulation of *Ebf2* expression during differentiation (15) has made it difficult to identify differentiated cells generated from *Ebf2*$^+$ progenitors in the BM. In order to investigate the contribution of *Ebf2*$^+$ cells to cellular components in the BM *in vivo*, we adopted a lineage-tracing strategy using a BAC transgenic mouse model where the regulatory elements from the *Ebf2* gene drive expression of a Cre-recombinase protein were fused to a modified estrogen receptor to allow for a tamoxifen-controlled import of the recombinase into the nucleus (Fig. 1A). These mice were crossed with a mouse strain carrying the *Yfp* gene under the control of the regulatory elements of the ubiquitously expressed *Rosa26* gene (32) and a stop cassette flanked by lox sites allowing for a permanent labeling of *Ebf2*-expressing cells and their progeny upon injection of tamoxifen (Fig. 1A). We examined the presence of Cre- and YFP-expressing cells in BM sections from the bitransgenic [Tg(*Ebf2*-CreER × Rosa26-*Yfp*)] mice at 11 to 32 weeks after tamoxifen treatment. In addition to individual cells with Cre expression (Fig. 1B and C), we could observe clusters of YFP$^+$ cells (five to six clusters in 20 femur sections) at 11 weeks after tamoxifen treatment (Fig. 1D and E). A higher number of the YFP$^+$ cell clusters were observed at 32 weeks after treatment. The majority of the clusters were located in proximity to the bone surface (Fig. 1D) and in articular cartilage (Fig. 1F). To determine cellular identity of the YFP$^+$ cells, we analyzed the coexpression of YFP and the osteoblast marker osteocalcin or chondrocyte marker aggrecan in the cells. We could detect a number of YFP$^+$ aggrecan$^+$ cells in the epiphysis line and articular cartilage of femurs (Fig. 1F to H). The YFP$^+$ osteocalcin$^+$ cells were observed in the endosteal area (Fig. 1I). These data suggested that the physiological contribution of the *Ebf2*$^+$ cells to both osteoblasts and chondrocytes, indicating that they are not predestined to osteoblastic lineage development and opening the possibility that they represent multipotent progenitors in the adult BM.

Preferential location of the *Ebf2*-expressing cells in the BM endosteal region. In order to prospectively isolate the *Ebf2*$^+$ cells, we utilized a transgenic mouse model where the regulatory elements of the *Ebf2* gene directly drives the expression of GFP (Tg *Ebf2*-Egfp), allowing us to isolate the *Ebf2*$^+$ cells by FACS. We found that GFP/*Ebf2*$^+$ cells accounted for 0.002% ± 0.0007% of total BM nucleated cells exclusively resided in the nonhematopoietic CD45$^-$ TER119$^-$ BM cell fraction (Fig. 2A). Quantitative PCR analysis of *Ebf2* expression in the sorted CD45$^-$ LIN$^-$ GFP$^{+/-}$ cells showed that while *Ebf2* was easily detected in the GFP$^+$ cells, the expression in GFP$^-$ cells was low or undetectable, indicating a high fidelity of GFP expression to that of the endogenous *Ebf2* gene (Fig. 2B and C). To investigate the anatomical location the *Ebf2*$^+$ cells in adult BM, the cells were collected from

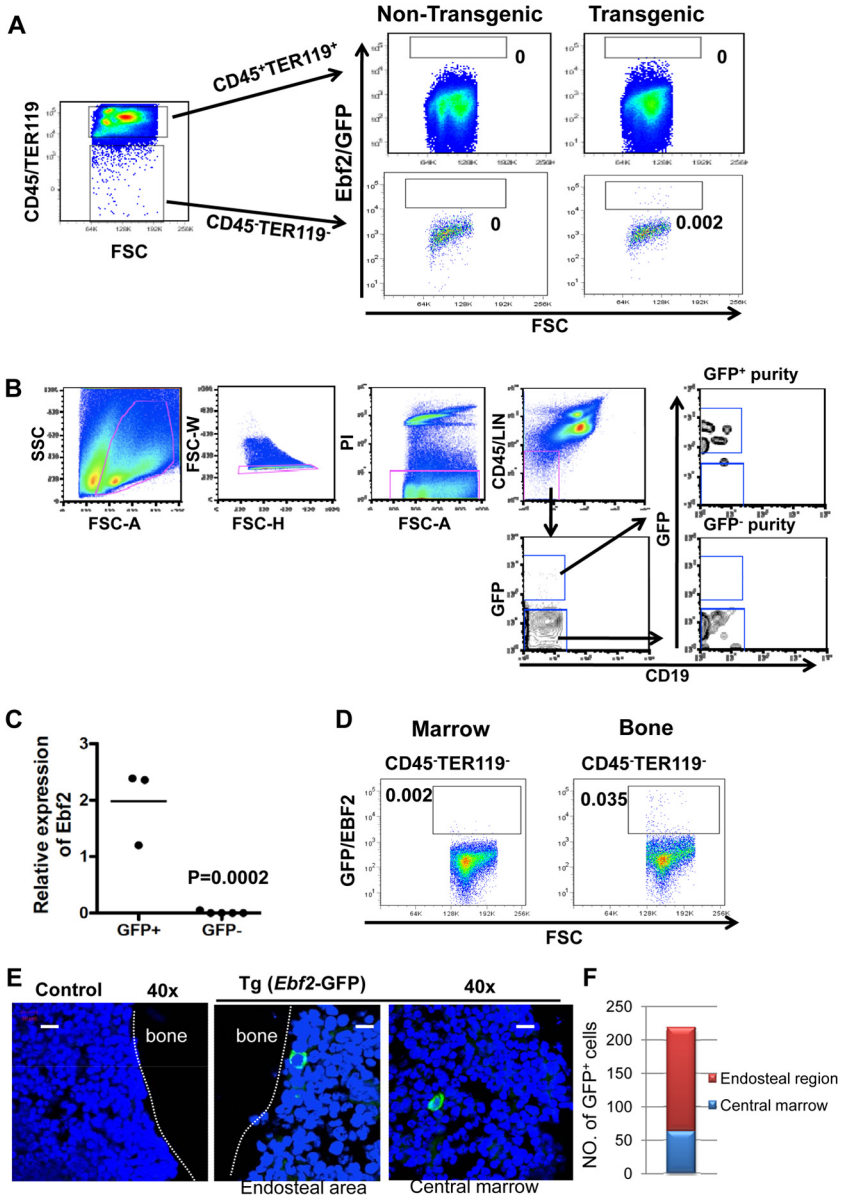

FIG 2 Unique expression of *Ebf2* in the nonhematopoietic BM cells. (A) *Ebf2* is selectively expressed in nonhematopoietic CD45$^-$ TER119$^-$ BM stromal cell compartment in mouse BM. The hematopoietic cells (CD45$^+$ TER119$^+$) and nonhematopoietic CD45$^-$ TER119$^-$ cells were first gated within PI$^-$ live cells, and GFP$^+$ cells were gated within these two cell compartments based on the control staining on BM cells from nontransgenic mice. The numbers in the panels are the mean frequencies of gated cells of total viable cells ($n = 3$). The data are from one representative experiment of two with similar results. (B) FACS sorting strategy of CD45$^-$ TER119$^-$ GFP$^{+/-}$ cells from BM. The dead cells and doublets were excluded using FSC height (FSC-H) versus FSC width (FSC-W) and subsequently by PI staining. Since our preliminary investigation indicated that the most probable contaminating cells were CD19$^+$ B-lineage cells, we included CD19 on a separate channel. GFP$^+$ cells were gated according to FMO controls using BM cells from nontransgenic mice. (C) Quantitative PCR analysis of *Ebf2* expression in the sorted GFP$^{+/-}$ cells. The expressions of *Ebf2* were normalized to that of *Hprt* in each of the cell types. Each dot represents a mean value of the triplicate measurements in each experiment. The data are from three independent experiments. (D) FACS analysis of frequencies of CD45$^-$ TER119$^-$ GFP$^+$ cells in unfractionated cells from marrow (left) and bone endosteal region (right). The bone endosteal cells were obtained by collagenase and trypsin treatment after removal of the marrow cells. The numbers are mean frequencies of the GFP$^+$ cells of total mononuclear cells ($n = 2$). (E) Distribution of the GFP$^+$ cells in adult BM. Left, control staining; right, GFP$^+$ cells in the marrow and endosteal regions. Blue indicates DAPI-stained nuclei. Scale bars, 10 μm. (F) The numbers of GFP$^+$ cells located in endosteal region and in the central marrow. The endosteal region and central marrow (>12 cells from bone surface) was defined as described previously (33). A total of 219 GFP$^+$ cells were counted from 41 consecutive femur sections from four mice. The data are from three experiments.

the central BM cavity after gently crushing of the bone and from the endosteal region by subsequent enzyme treatment (trypsin and collagenase) of the bone fragments. FACS analysis of the two cell preparations showed that the frequency of CD45$^-$ TER119$^-$ GFP$^+$ cells in the endosteal cells was 12-fold higher than that in the marrow cell preparation (Fig. 2D), suggesting that the GFP$^+$ cells are preferentially enriched in the endosteal cells of BM. The results were confirmed by the *in situ* staining of bone sections from the *Ebf2* transgenic mice because 75% of the GFP/*Ebf2*$^+$ cells were located in the endosteal region (<12 nuclei from the bone

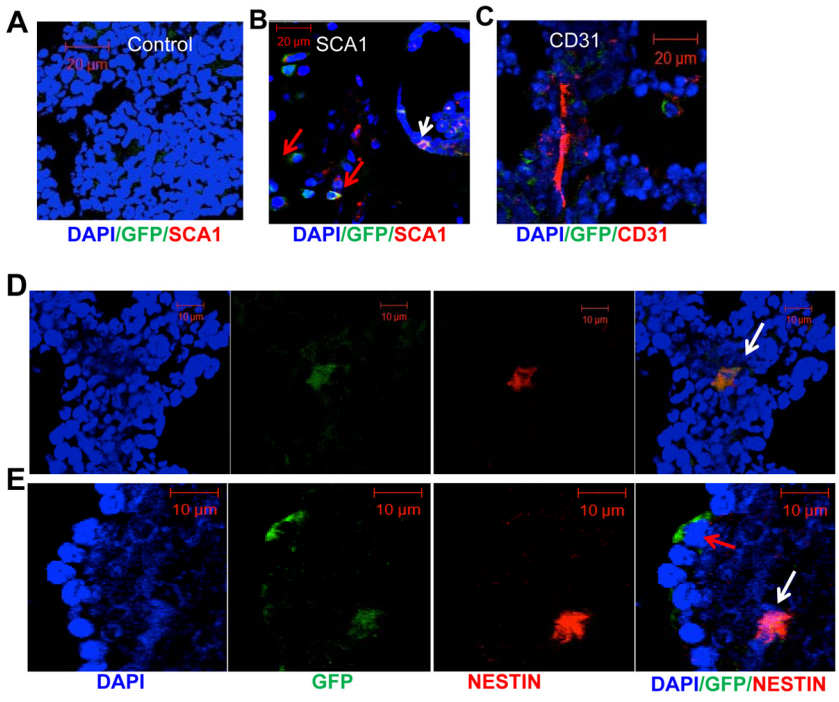

F

Cell types	Cell number	% of total *Ebf2*$^+$ cells
Ebf2$^+$SCA1$^+$	57	35.4
Ebf2$^+$SCA1$^-$	104	64.6
Ebf2$^+$Nestin$^+$	64	59.8
Ebf2$^+$Nestin$^-$	43	40.2

FIG 3 *In situ* expression analysis of SCA1, CD31, and nestin in femur sections of adult Tg *Ebf2-Egfp* mice. Nuclei were counterstained with DAPI. (A) Control staining for SCA1, CD31, and nestin. The section was stained with only secondary antibodies. (B) Coexpression of SCA1 with *Ebf2*/GFP in the trabecular femur. A white arrow indicates the cell positive for *Ebf2* and SCA1, and red arrows indicate the Ebf2$^+$ SCA1$^-$ cells. (C) The was no close association of Ebf2$^+$ cells (green) with CD31$^+$ cells (red). (D and E) Coexpression of nestin with *Ebf2*/GFP in trabecular femur. A white arrow indicates a nestin$^+$ *Ebf2*$^{+/low}$ cell, and a red arrow indicates the cell expressing *Ebf2* only. (F) Numbers of *Ebf2*$^+$ cells expressing SCA1 or nestin in mouse femur sections. The data were from the femoral sections of two mice.

surface) (33) (Fig. 2E and F). Hence, *Ebf2* expression is confined to a small fraction of stromal cells enriched in the endosteal region.

Expression of MSC-associated markers in the *Ebf2*$^+$ cells. Physiological contribution to both osteoblasts and chondrocytes and anatomical location in BM endosteal region of the *Ebf2*$^+$ cells prompted us to investigate whether these cells express MSC-associated markers. SCA1 and *Nestin* have been recently shown to be expressed in mouse BM MSCs (10, 11, 13). We found that ca. 35.4 and 59.8% of the *Ebf2*$^+$ cells expressed SCA1 and nestin, respectively (Fig. 3). Most of the *Ebf2*$^+$ cells residing in the bone did not express SCA1, while the cells located in endosteal area or marrow did (Fig. 3B). Around 60% of the *Ebf2*$^+$ cells, albeit at a relatively low level, express nestin (Fig. 3D to F). This finding is in consistent with the previous reports about expression of SCA1 and nestin on mouse MSCs (10, 11). However, we could only detect few pericyte-like *Ebf2*$^+$ cells by costaining of GFP with the arteriole marker SCA1 (34), revealing that majority of the *Ebf2*$^+$ cells are not adjacent to vascular endothelial cell layer (Fig. 3C).

Primary BM MSCs has been reported to express CD105, SCA1, PDGFRα, CD90, and CD51 (14, 35–39) but are negative for CD44 (14), whereas osteoblast progenitors lack SCA1 expression (40). Multicolor FACS analysis revealed that the majority of the *Ebf2*$^+$ cells expressed CD105, PDGFRα, CD90, CD51, and SCA1, while lacking expression of CD44 and CD31 (Fig. 4A). The frequency of SCA1$^+$ *Ebf2*$^+$ cells (82% ± 10%) detected by FACS is ~2-fold higher than that detected by *in situ* fluorescent staining (Fig. 3F). This discrepancy could be explained by a combination of a higher sensitivity in SCA1 detection in flow cytometry and that we have during the preparation of cells for flow cytometry intentionally excluded cells from the epiphysis line and articular cartilage. In all, the *Ebf2*-expressing cells of the BM phenotypically resemble a MSC population.

***Ebf2*-expressing cells are physiologically quiescent.** Quiescence is a common feature of adult tissue stem cells under steady state and has been suggested to serve as a means to maintain the stem cell properties over time (1, 41–43). Our cell cycle analysis by

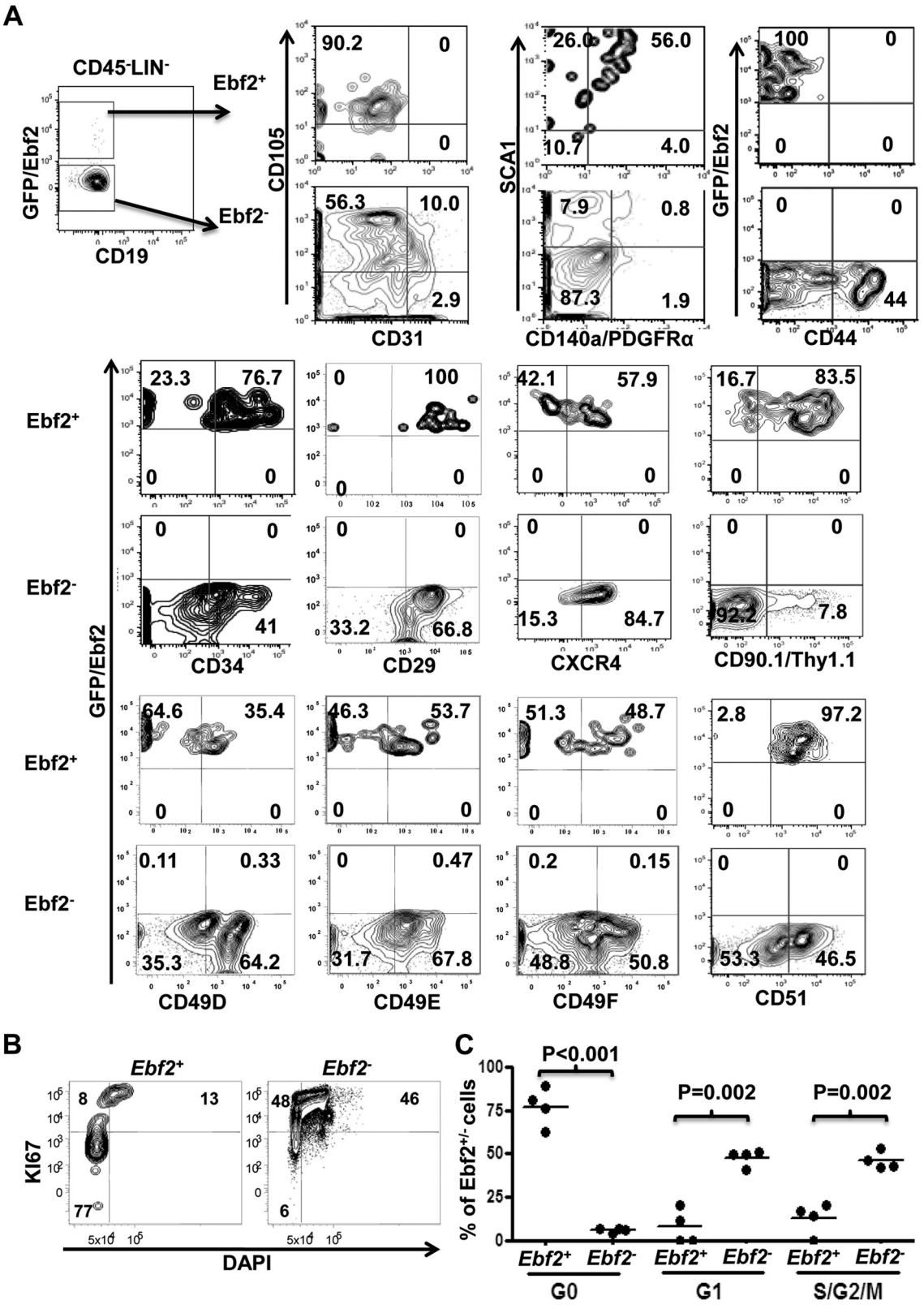

FIG 4 Cell surface marker expression in the *Ebf2*-expressing cells and cell cycle status of the cells. (A) Cell surface marker expression profile of the *Ebf2*$^+$ cells. The cells recovered from hematopoietic cell depletion were stained with CD45 and lineage (LIN, TER119/CD4/CD8/MAC1/GR1/B220) antibodies. Around 500,000 to 1.5 million nucleated cells in total were collected for the analysis. The *Ebf2*$^+$ and *Ebf2*$^-$ cells were gated within CD45$^-$ LIN$^-$ cells according to FMO FITC in which BM cells from nontransgenic mice were used. The expressions of CD31, CD105, SCA1, CD140a/PDGFRα, CD34, CD44, CD29, CD49D, CD90.1/Thy1.1, CD49E, and CD49F on the GFP/*Ebf2*$^+$ cells are displayed as indicated. The numbers in the panels are mean percentages of the positive cells of gated *Ebf2*$^+$ and *Ebf2*$^-$ cells. The data were from at least two experiments. (B and C) Cell cycle analysis of the GFP/*Ebf2*$^+$ cells by FACS. (B) FACS profiles of cell cycle analysis of the GFP/*Ebf2*$^+$ cells by KI67 and DAPI staining. Cell cycle status within defined *Ebf2*$^+$ and *Ebf2*$^-$ subsets was determined by simultaneous two-parameter analysis with DNA content versus KI67 expression. Numbers in the quadrants indicate the percentages of gated cells in each of the cell cycle phases (G_0, G_1, and $S/G_2/M$). (C) Mean cell cycle distribution of total *Ebf2*$^+$ and *Ebf2*$^-$ cells from two experiments.

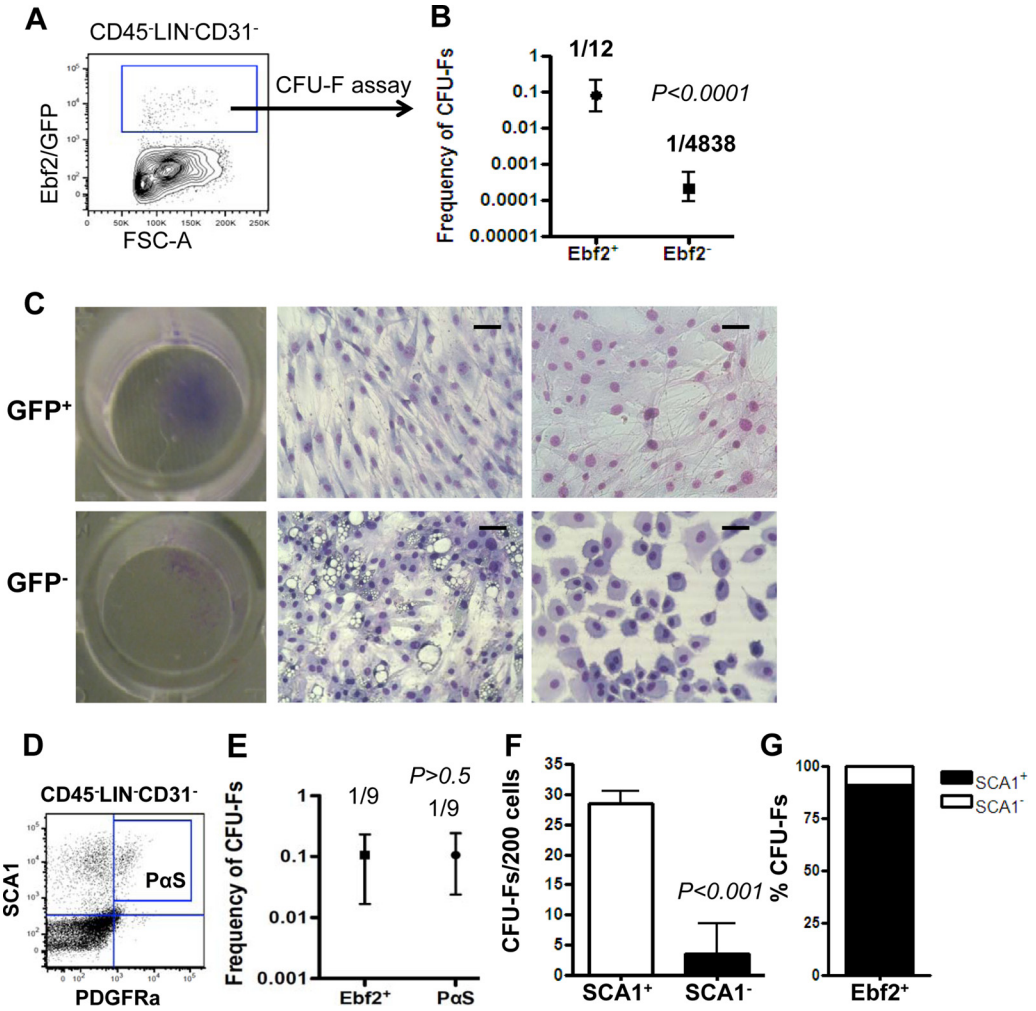

FIG 5 CFU-Fs are highly enriched in *Ebf2*$^+$ cells. (A) Representative FACS profile showing the sorting strategy to purify CD45$^-$ LIN$^-$ GFP/*Ebf2*$^{+/-}$ cell and the purities of the sorted cells. The cells recovered from hematopoietic cell depletion were stained with CD45 and lineage antibodies and used for cell sorting. The cells were first gated from PI$^-$ cells, and the gate for GFP$^+$ cells within CD45$^-$ LIN$^-$ cell compartment was based on the FMO control using BM from a nontransgenic mouse. (B) Frequency of CFU-Fs in GFP$^{+/-}$ cells, calculated using L-Calc (Stem Cell Technologies). The cells were cultured under normoxic condition (21% O_2). The data are mean ± the 95% confidence interval from three independent experiments. (C) Morphology of Giemsa-stained CFU-Fs derived from the GFP$^+$ (upper) and GFP$^-$ (lower) cells. Scale bars, 25 μm. (D) Sorting of PαS cells. (E) CFU-F frequencies in PαS cells and *Ebf2*$^+$ cells. The two cell types were sorted and seeded at 2, 5, 10, and 20 cells/well for the CFU-F assay. The frequencies of CFU-Fs were calculated using L-Calc. The data are means ± the 95% confidence interval from two independent experiments. ns, no significant difference. (F and G) The CFU-F activity in *Ebf2*$^+$ cells is restricted to the SCA1$^+$ cell subfraction. The data are from four independent experiments. (F) Numbers of CFU-Fs per 200 *Ebf2*$^+$ SCA1$^+$ and *Ebf2*$^+$ SCA1$^-$ cells. (G) Distribution of CFU-Fs in *Ebf2*$^+$ SCA1$^+$ and *Ebf2*$^+$ SCA1$^-$ cells (% of total).

FACS revealed that the majority of the *Ebf2*$^+$ cells resided in the G_0 phase (>70%) and correspondingly fewer GFP/*Ebf2*$^+$ cells were at the G_1 and S/G_2/M phases. In contrast, the majority of the GFP/*Ebf2*$^-$ cells were either in the G_1 or the S/G_2/M phase and thus displayed an active cell cycle status (Fig. 4B and C). The data suggest that the majority of the *Ebf2*$^+$ cells physiologically reside in a quiescent state.

***Ebf2*-expressing cells are highly enriched for CFU-Fs.** To functionally characterize the *Ebf2*-expressing cells, we performed a limiting dilution assay to estimate the CFU-F activity in freshly sorted CD45$^-$ LIN$^-$ *Ebf2*$^+$ cells and *Ebf2*$^-$ cells (Fig. 5A and B). The frequency of CFU-Fs in the *Ebf2*$^+$ cells was 1/12 under normoxic condition, 400-fold higher than the frequency of 1/4,838 in the *Ebf2*$^-$ cells (Fig. 5B). The CFU-Fs derived from the *Ebf2*$^+$ cells were typically larger and more fibroblast-like than those from the *Ebf2*$^-$ cells (Fig. 5C). Using hypoxic conditions, reported to be important for maintaining stem cell properties (44), allowed us to obtain a cloning frequency of 1/9 cells, similar to what we observed for PαS (PDGFRα$^+$ SCA1$^+$) cells (Fig. 5D and E). The CFU-F activity was further enriched in *Ebf2*$^+$ cells expressing SCA1 (Fig. 5F and G).

Single cell analysis and transplantation provides evidence for the multipotency of *Ebf2*$^+$ cells. Since our lineage-tracing experiments and phenotypic as well as functional characterization suggested that the *Ebf2*$^+$ cells are not restricted to osteoblast development *in vivo*, we wanted to further investigate multilineage differentiation potentials of the *Ebf2*$^+$ cells at single cell level. To this end, we collected cells from a single CFU-F generated in the limiting dilution assays and split the cells from the single clone into the media to induce differentiation of adipocytes (AD),

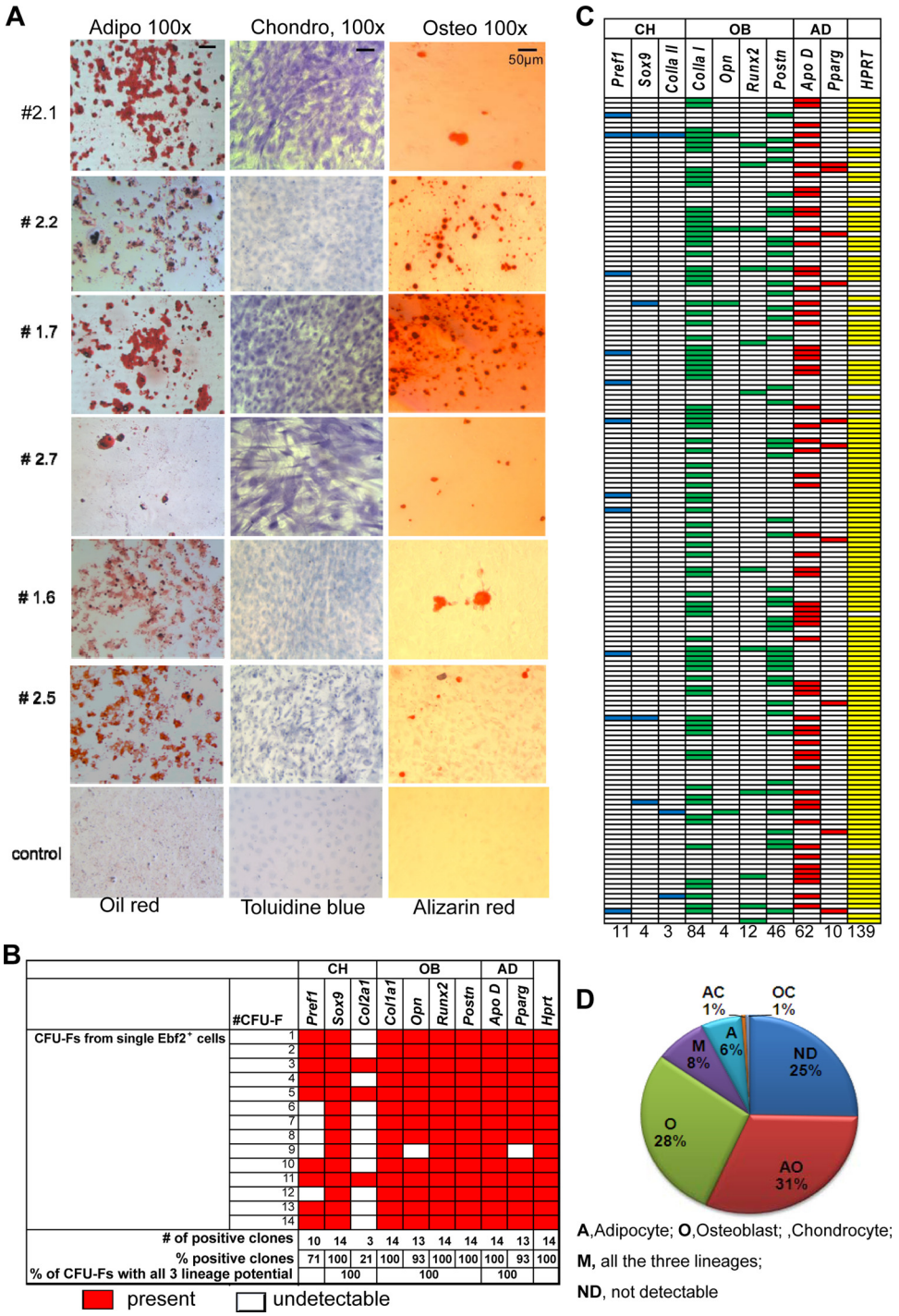

FIG 6 *Ebf2*$^+$ cells display multilineage differentiation potential. (A) Differentiated osteoblasts, adipocytes, and chondrocytes generated from single *Ebf2*$^+$ cell clones. The cell clones were picked from single CFU-Fs derived the single *Ebf2*$^+$ cells that were freshly sorted and plated in a 96-well plate in limiting dilution assays. The numbers beside the images are clone number. The expanded cells were used for *in vitro* differentiation of adipocytes, chondrocytes, and osteoblasts. The chondrocyte differentiation was induced in monolayer culture in chondrogenic medium. The cells were cultured in adipogenic, chondrogenic, and osteogenic induction media for 21 to 28 days and then stained with oil red, toluidine blue, and alizarin red. (B) Multiplex RT-PCR analysis of multiple lineage-associated genes in a single *Ebf2*$^+$ cell-derived CFU-F. Every row represents one CFU-F, and a red square indicates that mRNA from the gene could be detected as a band on an ethidium bromide-stained agarose gel. The colonies were scored as expressing CH-, AD-, and/or OB-associated genes based on the expression of one or more lineage-associated genes ($n = 14$). (C and D) Single-cell RT-PCR analysis of lineage-associated genes in single *Ebf2*$^+$ cells. The cells were sorted in 96-well plates at 1 cell/well and subjected to single cell multiplex RT-PCR analysis for expression of multiple lineage-associated genes. The blue, green, red, and yellow squares in panel C indicate that an RT-PCR product for an indicated gene could be detected on an ethidium bromide-stained agarose gel. Each row represents a single cell. The numbers at bottom of the panel indicate the number of cells expressing the indicated gene. (D) Percentages of the *Ebf2*$^+$ cells expressing multilineage or specific lineage-associated genes. The cells were scored as expressing chondrocyte, adipocyte, and/or osteoblast genes based on the expression of one or more lineage-associated genes.

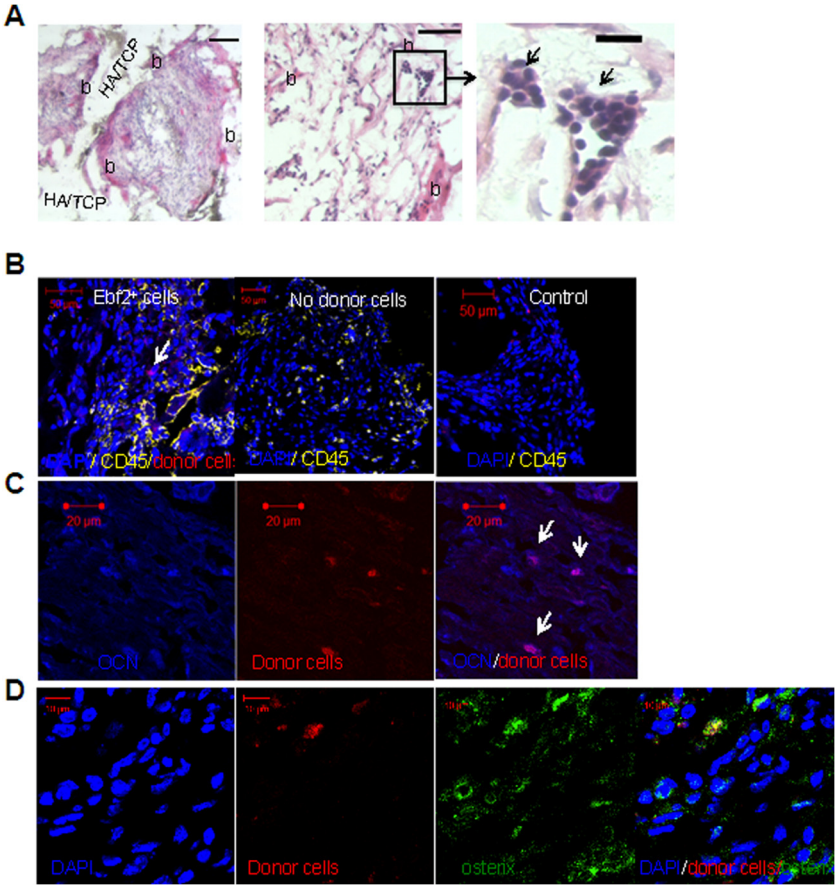

FIG 7 *In vivo* differentiation of the *Ebf2*$^+$ cells 6 to 7 weeks after heterotopic transplantation. The culture-expanded *Ebf2*$^+$ cells labeled with mStrawberry were loaded into ceraforms (HA/TCP) and transplanted subcutaneously under the dorsal skin of normal adult FVB/N mice. The data are from one representative experiment of three. (A) H&E-stained transplanted ceraforms showing colocalization of hematopoietic areas with bone matrix. The pink area indicates bone matrix formation (arrows). Scale bar, 250 μm. Hematopoietic cell clusters in the ossicles are shown in middle and right panels (enlarged). The "b" indicates bone formation. Scale bars, 100 μm (middle) and 25 μm (right). (B) Colocalization of CD45$^+$ cells with donor-derived cells in the ceraform. Red indicates the donor cell type, yellow indicates CD45 expression, and blue indicates DAPI staining of cell nuclei. (C and D) Donor-derived osteocalcin$^+$ (OCN$^+$) cells (blue and red) (C) and osterix$^+$ cells (green and red) (D) in the ceraforms.

osteoblasts (OB), or chondrocytes (CH). Three to four weeks after the initiation of the induction, all eight investigated single clones generated differentiated AD, OB, and CH cells that were identified by oil red S, alizarin red, and toluidine blue staining, respectively (Fig. 6A). Furthermore, we performed nested RT-PCR analysis of multilineage-associated genes in the single CFU-F generated from a single freshly sorted *Ebf2*$^+$ cell in the limiting dilution assays. The genes included were *Pref1*, *Sox9*, and *Col2a1*, all associated with chondrocyte development, *Col1a1*, *Opn*, *Runx2*, and *Periostin*, which are linked to osteoblastic lineages, and the adipocyte-associated genes *ApoD* and *Pparg* (11, 28, 45). Of 14 CFU-Fs analyzed, all of the clones expressed genes associated with all of the three lineages (Fig. 6B). These data clearly indicate the multilineage differentiation potentials of the single *Ebf2*$^+$ cell clones *in vitro*.

The concept of multilineage-priming was first established in the hematopoietic stem cell compartment (26, 27) and appears to represent a common theme in several stem cell populations, including MSCs (45). To investigate whether the *Ebf2*$^+$ cells are bona fide multilineage primed, we examined the coexpression of lineage-associated genes in 166 freshly sorted *Ebf2*$^+$ cells (1 cell/well in a 96-well format) by multiplex single cell-PCR (26, 27), allowing us to analyze the coexpression of multiple genes in a single cell *ex vivo*. In 8% of the cells, we detected simultaneous expression of OB-, CH-, and AD-associated genes (Fig. 6C and D), indicating genuine multilineage priming in a fraction of the cells. Even though this assay is likely to be biased by low expression levels of genes, resulting in failure of detection, the finding that lineage-associated genes are coexpressed in a fraction of the primary cells provides evidence for genuine multilineage-priming at the single cell level.

In vivo bone formation ability of the *Ebf2*$^+$ cells was examined by heterotopic transplantation of the single *Ebf2*$^+$ cell clones. The cells were stably labeled by retroviral transduction with a retrovirus expressing mStrawberry fluorescent protein. The cells were loaded into ceramic ossicles (ceraforms) and transplanted subcutaneously into normal adult FVB/N mice. Bone formation, fibroblastic tissue, and hematopoietic activity could be detected in the ceraforms at 6 to 7 weeks after transplantation (Fig. 7A). Donor-derived osteoblasts expressing mStrawberry and osteocalcin or osterix (Fig. 7B to D) were observed in the transplants, suggesting *in vivo* osteoblast differentiation capacity of the *Ebf2*$^+$ cells.

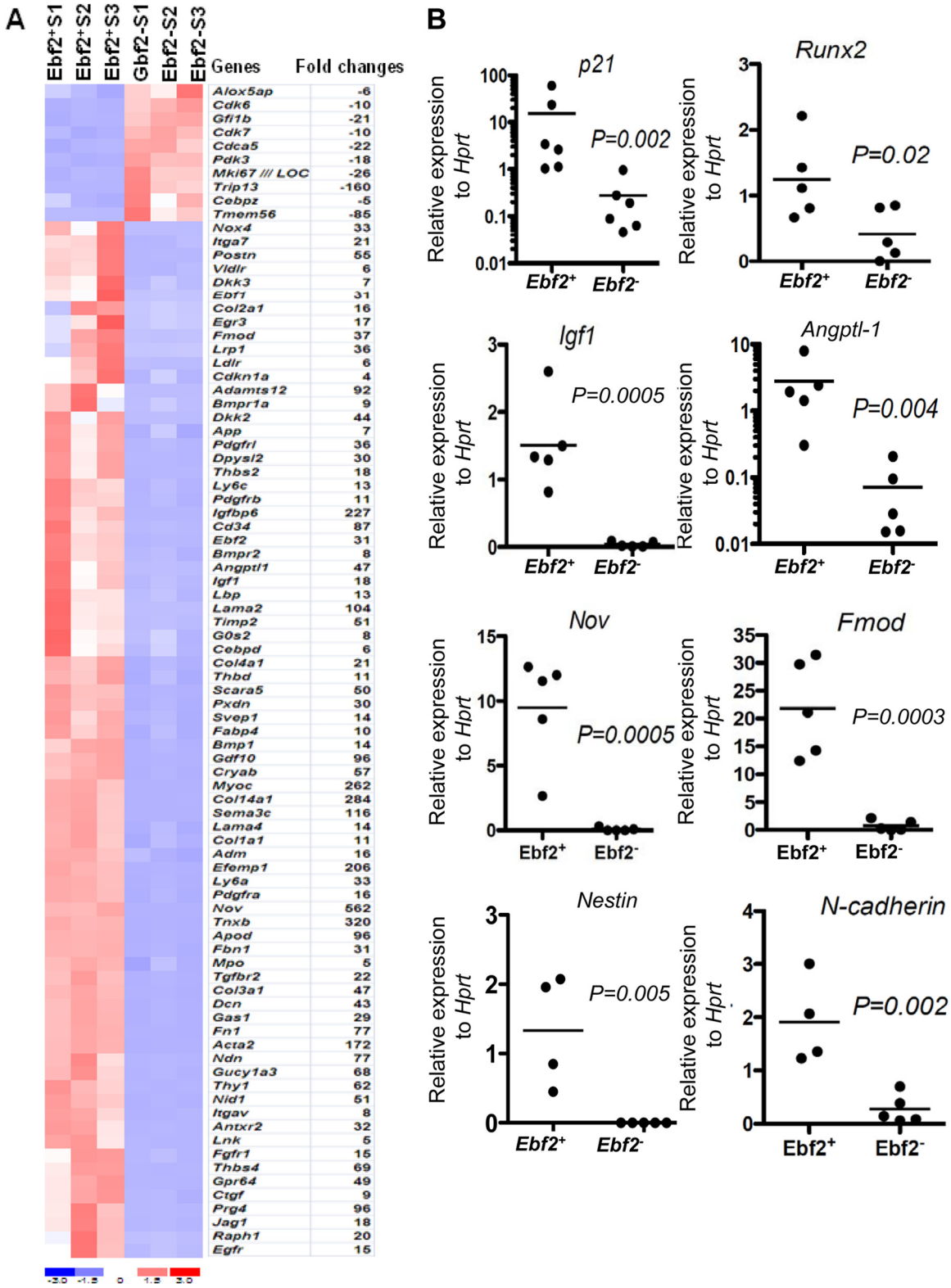

FIG 8 Molecular features of the *Ebf2*$^+$ and *Ebf2*$^-$ cells. (A) dCHIP analysis of global gene expression in CD45$^-$ LIN$^-$ GFP$^+$ cells and GFP$^-$ cells. Clustering shows genes being up- or downregulated 4-fold in the GFP$^+$ cells compared to the GFP$^-$ cells. Red represents high and blue represents low expression. The data were from three independent microarray experiments. (B) RT-PCR analysis of *Nov*, *Fmod*, *Igf1*, *Runx2*, *N-cadherin*, *Angiopoietin-like 1*, *Nestin*, and *p21* in sorted *Ebf2*$^+$ and *Ebf2*$^-$ cells. The differences between the two cell populations were compared by unpaired Student *t* test. The data were from five to six independent sorting experiments. Each dot represents mean of triplicate measurements in each experiment.

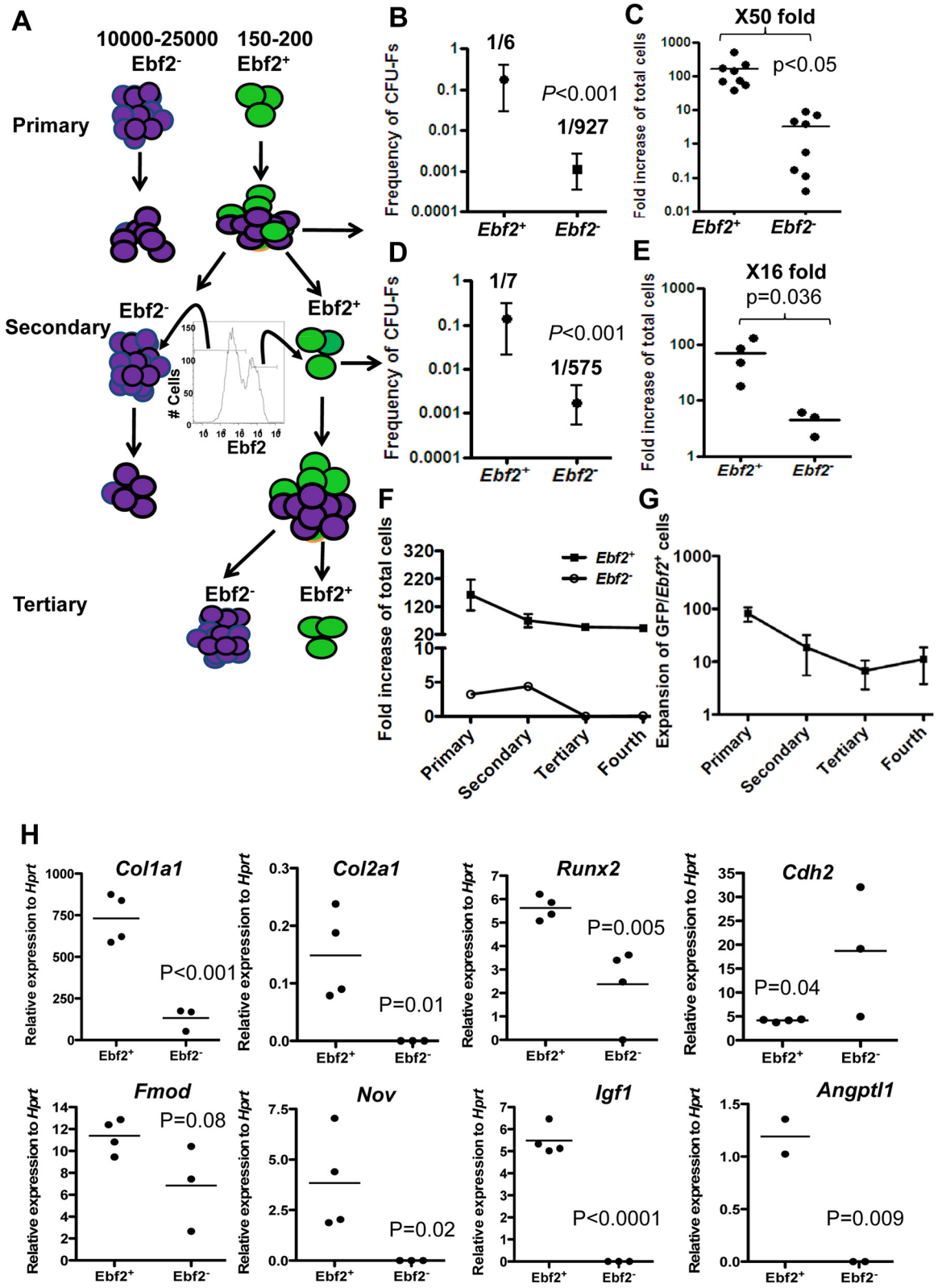

FIG 9 *Ebf2*-expressing cells display self-renewal capacity during *in vitro* serial replatings. (A) Experimental layout of self-renewal analysis. BM CD45$^-$ LIN$^-$ *Ebf2*/GFP$^{+/-}$ cells were sorted and seeded at a density of 150 to 200 cells/well for the *Ebf2*$^+$ fraction and 10,000 to 25,000 cells/well for the *Ebf2*$^-$ fraction in a 12-well plate. The daughter GFP/*Ebf2*$^+$ and GFP/*Ebf2*$^-$ cells were then sorted at each passage for further serial replatings. (B and D) The frequency of CFU-Fs derived from freshly isolated (B) or expanded (D) *Ebf2*$^+$ and *Ebf2*$^-$ cells. Limiting dilution assay of CFU-Fs in the expanded GFP$^+$ and GFP$^-$ cells at the first passage was performed at the cell doses of 1, 2, and 5 cells/well for the GFP$^+$ cells and 100 cells/well for the GFP$^-$ cells. The frequencies of CFU-Fs were calculated and the differences between the *Ebf2*$^+$ and *Ebf2*$^-$ cells were compared by using the Student *t* test built in L-Calc software (Stem Cell Technologies). (C and E) Fold

Global gene expression analysis provides molecular insights to the genetic programs defining the MSCs. The ability to prospectively isolate highly purified MSCs provided us with an opportunity to characterize the molecular nature of the cells. To identify the true molecular features of the *Ebf2*$^+$ cells, we performed microarray analysis of freshly sorted CD45$^-$ TER119$^-$ *Ebf2*$^+$ and *Ebf2*$^-$ cells (Fig. 8A). This allowed for the detection of 1968 genes that were 2-fold differentially expressed in *Ebf2*$^+$ and *Ebf2*$^-$ cells. Among these, 1,075 genes were upregulated and 893 genes, including *Ebf2*, were downregulated in the *Ebf2*$^-$ compared to the *Ebf2*$^+$ cells. These include *Nov*, *Fmod*, *Ndn*, *Dcn*, *Ctgf*, *Angiopoietin-like 1* (*Angptl1*), *Fn1*, and *Jag1* (Fig. 8), some of which has been reported to be expressed in culture-selected MSCs (4, 46, 47). Furthermore, consistent with antigen expression analysis by FACS, the *Ebf2*$^+$ cells highly expressed transcripts of *Pdgfra*, *Pdgfrb*, *Sca1/Ly6a*, *Thy1*, and *Itga7* and *Itgav* that have been suggested to be expressed by MSCs (11–13, 46, 47). *Nestin* was mainly expressed in *Ebf2*$^+$ cells, whereas it was hardly detectable in the *Ebf2*$^-$ cells (Fig. 8B). Altogether, molecularly, the *Ebf2*$^+$ cells displayed features of an MSC.

Single *Ebf2*$^+$ cell clones have the capacity to self-renew *in vivo*. To assess the self-renewal capacity of the *Ebf2*$^+$ cells, we performed serial replating of sorted *Ebf2*$^+$ and *Ebf2*$^-$ stromal cells (Fig. 9A). A total of 150 to 200 sorted *Ebf2*$^+$ cells and 10,000 to 25,000 *Ebf2*$^-$ cells were plated in 12-well plates in order to obtain relatively comparable numbers of cells at the end of the culture period of each passage and to avoid the development of confluent cultures in which cell proliferation could be affected by contact inhibition. The two cell populations also displayed a dramatic difference in proliferation capacity as the total number of the cells generated from the *Ebf2*$^+$ cells increased on an average 162-fold, whereas the number of cells from the *Ebf2*$^-$ cells were only slightly increased under the same conditions (Fig. 9C, E, and F). FACS analysis revealed that the *Ebf2*$^+$ cells generated both GFP/*Ebf2*$^+$ and GFP/*Ebf2*$^-$ cells, whereas no GFP$^+$ cells could be detected in the cultures generated from the *Ebf2*$^-$ cells (Fig. 9A and G). To determine whether the daughter *Ebf2*$^+$ cells retain the same clonogenic potential as their parental cells, we sorted the *Ebf2*$^{+/-}$ cells generated from the primary *Ebf2*$^+$ cells and performed limiting dilution assays of the CFU-Fs (1, 2, and 5 cells/well of the *Ebf2*$^+$ cells and 200 cells/well of the *Ebf2*$^-$ cells). The frequencies of CFU-Fs in cultured *Ebf2*$^{+/-}$ cells (Fig. 9D) were similar to those obtained from the CFU-Fs cultured in the freshly isolated *Ebf2*$^{+/-}$ cells (1/6 in the *Ebf2*$^+$ cells and 1/927 in the *Ebf2*$^-$ cells, on average) (Fig. 9B) ($P = 0.08$), suggesting that the clonogenic capacity remained in the expanded *Ebf2*-expressing cells. To test whether the expanded GFP/*Ebf2*$^+$ cells also maintained the molecular features of the primary *Ebf2*$^+$ cells, we compare gene expression patterns in the primary *Ebf2*$^+$ cells with the expanded *Ebf2*$^+$ cells. We found that the MSC-associated gene expression profile of the expanded GFP$^+$ cells, with the exception of N-cadherin (*Cdh2*), was very similar to that of the freshly isolated *Ebf2*$^+$ cells (Fig. 9H).

Sustainable expansion has been considered to reflect self-renewal capacity of stem cells. Thus, we examined the expansion capacity of *Ebf2*$^+$ cells during *in vitro* replatings. The GFP/*Ebf2*$^+$ and GFP/*Ebf2*$^-$ cells derived from the *Ebf2*$^+$ cells at the previous passage was sorted by FACS and replated. The total cell numbers in culture remain dramatically increased after secondary (Fig. 9E) and tertiary (Fig. 9F) replating of the expanded *Ebf2*$^+$ cells, suggesting that these cells display a high proliferative capacity *in vitro*. Based on the frequency of the expanded GFP/*Ebf2*$^+$ cells and the total number of cells in culture, we calculated the numbers of the expanded GFP/*Ebf2*$^+$ cells in cultures and found a dramatic expansion of pure *Ebf2*$^+$ cells (82-fold on average for the input *Ebf2*$^+$ cells in the primary culture and 6- to 12-fold expansion during later replatings) (Fig. 9G). Taken together, these data provided both functional and molecular evidence for the self-renewal capacity of the *Ebf2*$^+$ cells *in vitro*.

To assess the ability of *Ebf2*$^+$ cells to maintain their MSC phenotype *in vivo*, we performed heterotopic and intravenous transplantation of single *Ebf2*$^+$ cell clones labeled with mStrawberry and evaluated the CFU-F activity of donor-derived cells at 6 to 7 weeks after transplantation. The donor-derived stromal cells (CD45$^-$ TER119$^-$ CD31$^-$ mStrawberry$^+$) were detected in the ceraforms at a frequency of 0.05% ± 0.03% (Fig. 10A to C). Both GFP/*Ebf2*$^+$ and GFP/*Ebf2*$^-$ cells were detected in the donor-derived cells in the ceraforms, and a majority of the *Ebf2*$^+$ donor-derived cells express SCA1 (Fig. 10B) and contain CFU-Fs (Fig. 10D and E) that retained the capacity to differentiate into adipocytes, chondrocytes, and osteoblasts *in vitro* (Fig. 10F). Similarly, the donor-derived cells with CFU-F activity could also be detected in the recipient BM intravenous injection via tail vein (Fig. 10G to I). This finding, together with *in vivo* bone differentiation capacity of the cells, suggested that single *Ebf2*$^+$ cell clones could generate cells that maintain MSC features while generating mesenchymal lineages *in vivo*.

DISCUSSION

Even though MSCs in BM have been extensively characterized through work with culture-selected mesenchymal progenitors, the data obtained from cultured cells may not predict the true cellular identity of the cells. Hence, it is essential to prospectively isolate the cells in order to identify their *in vivo* properties. In the present study, we prospectively isolated *Ebf2*-expressing cells from adult mouse BM and showed that these cells functionally, phenotypically, and molecularly fulfill the criteria of MSCs.

The multipotency of the *Ebf2*$^+$ cells was demonstrated by *in vivo* lineage-tracing experiments, as well as by *in vitro* differentiation of single *Ebf2*$^+$ cell clones. Our lineage-tracing experiments demonstrated the physiological contribution of *Ebf2*$^+$ cells to os-

increase in total cells derived from *Ebf2*$^+$ and *Ebf2*$^-$ cells in primary (C) and secondary (E) cultures. The data are means ± the standard error of the mean from three to seven independent experiments. (F and G) Kinetics of the fold increase in total cells (F) or the daughter GFP$^+$ cell subsets (G) generated from *Ebf2*-expressing cells during *in vitro* serial replatings. The fold increase was calculated based on the percentage of GFP$^+$ cells, the total number of the expanded cells in culture, and the number of input GFP$^+$ cells. (H) The expression of *Ebf2* is associated with MSC phenotype. The diagrams display quantitative PCR analysis of expressions of *Nov*, *Fibromodulin* (*Fmod*), *Insulin growth factor 1* (*Igf1*), *Runx2*, *N-cadherin* (*Cdh2*), *Angiopoietin-like 1* (*Angptl1*), *Collagen I* (*Col1a1*), and *Collagen II* (*Col2a1*) in the progeny-derived from *Ebf2*$^+$ cells derived progeny. *Ebf2*$^+$ and *Ebf2*$^-$ cells were observed in the culture seeded with freshly sorted *Ebf2*$^+$ cells and then were sorted by FACS at days 9 to 10 after culture for quantitative PCR analysis. The data are mean values of triplicate measurements obtained from two to three experiments. The differences between the two cell populations were compared by unpaired *t* test or Mann-Whitney test.

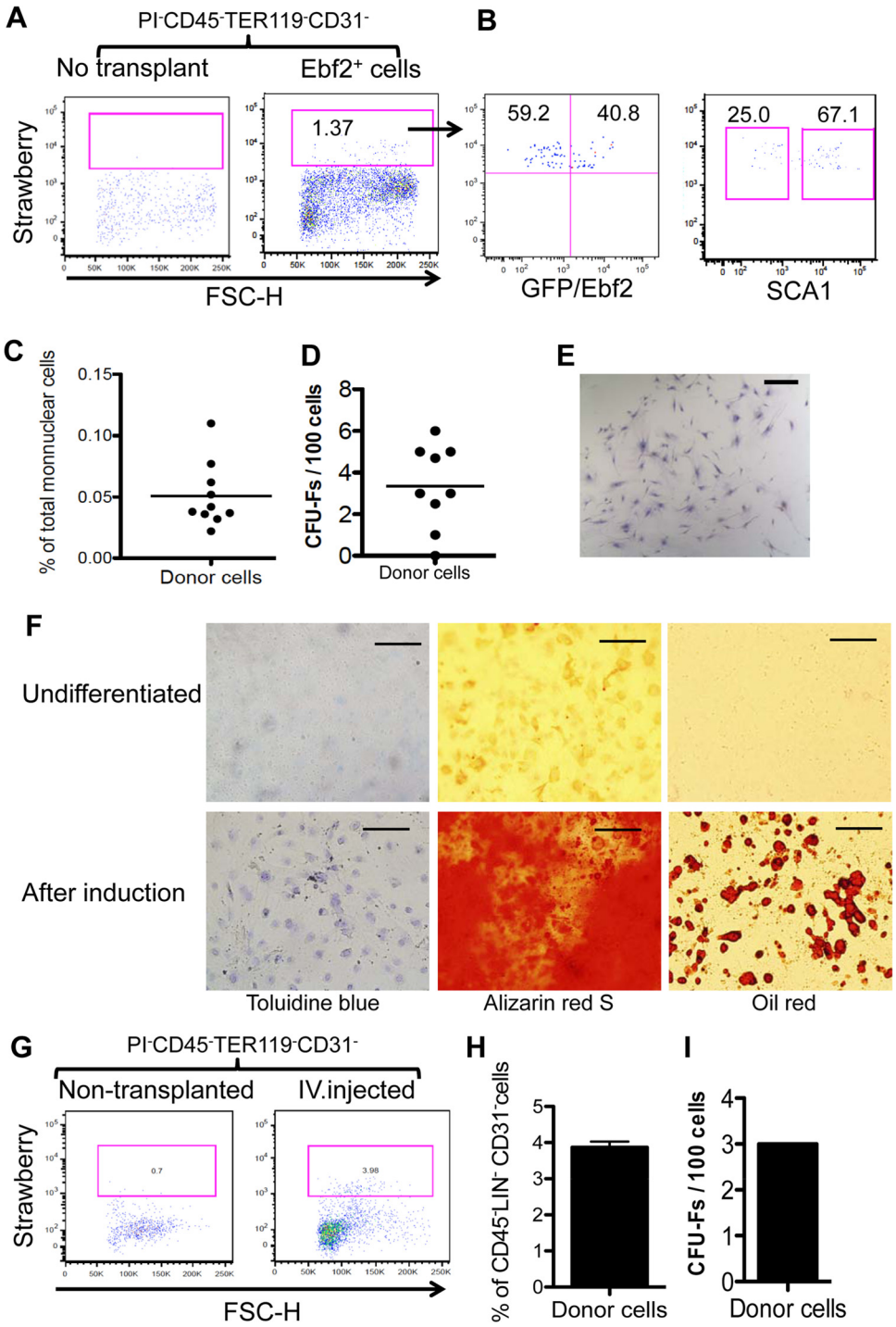

FIG 10 *Ebf2*-expressing cells self-renew *in vivo*. Ceraforms loaded with single *Ebf2*$^+$ cell clones were implanted subcutaneously under dorsal skin of 8- to 10-week-old normal FVB/N mice. The ceraforms were harvested at 6 to 7 weeks after transplantation. (A) Representative FACS profiles of donor-derived mStrawberry$^+$ cells. Around 100,000 to 400,000 nucleated cells in total were collected from each ceraform. The cells were first gated within CD45$^-$ TER119$^-$ CD31$^-$ cells. The gate for donor cells was defined based on the cells detached from control ceraforms (left) that were not preloaded with the donor cells. (B) Donor-derived cells expressing GFP/*Ebf2* (left) and SCA1 (right). The numbers in the panels are mean frequencies of the gated cell populations. (C) Frequency of the donor-derived cells in the total nucleated cells from the ceraforms. The data are from four experiments. (D) CFU-F activity of the sorted mStrawberry$^+$ donor cells. The data are from five experiments. (E) Morphology of CFU-F derived from donor cells. Scale bar, 500 μm. (F) *In vitro* multilineage differentiation of a donor-derived *Ebf2*$^+$ cell clone. The cells expanded from a single donor *Ebf2*$^+$ cell clone were induced in the respective differentiation media for 21 days. The differentiated adipocytes, osteoblasts, and chondrocytes were then stained by oil red O, alizarin red, and toluidine blue, respectively. Scale bars, 500 μm. (G to I) The *Ebf2*-expressing cells self-renew during intravenous transplantation. The culture-expanded *Ebf2*$^+$ mStrawberry$^+$ cells were transplanted via tail vein into 12- to 14-week-old sublethally irradiated (6 Gy) FVB/N mice. The bones were harvested at 6 weeks after transplantation for FACS analysis. (G) Representative FACS profiles of donor-derived mStrawberry$^+$ cells in the recipient BM (right panel). The cells were first gated within CD45$^-$ TER119$^-$ CD31$^-$ live cells. The donor cells were defined based on the cells from nontransplanted mouse BM (left). The right panel shows majority of the donor-derived cells express SCA1. The numbers in the panel are frequency of the gated cell populations. (H) Frequency of the donor-derived cells in the BM stromal cells (CD45$^-$ TER119$^-$ CD31$^-$; $n = 2$). (I) CFU-F activity of the sorted mStrawberry$^+$ donor cells. The cells were sorted from two recipient mice in one experiment.

teoblasts and chondrocytes defined by YFP$^+$ cell clusters expressing osteocalcin or aggrecan. Interestingly, the frequency of individual *Ebf2*-expressing cells identified by Cre expression in the double-transgenic mice is similar to that of GFP$^+$ cells in Tg *Ebf2-Egfp* reporter mice, indicating the maintenance of *Ebf2*$^+$ cells. The relatively low number of YFP$^+$ cell clusters in the BM likely reflects the fact that the majority of the *Ebf2*$^+$ cells are physiologically quiescent (77% of the cells reside in G_0 in the present study). Meanwhile, we have detected the coexpression of multiple lineage-associated genes, including *Sox9*, *Col2a1*, *Col1a1*, *Postn*, *ApoD*, and *Fabp4*, in a primary colony derived from a single *Ebf2*$^+$ cell, as well as in single freshly isolated progenitors, which suggests bona fide multilineage priming of a fraction of *Ebf2*$^+$ cells. The fraction of the multilineage-priming *Ebf2*$^+$ cells was similar to that of CFU-Fs in *Ebf2*$^+$ cells. These data, together with the *in vivo* contribution of *Ebf2*$^+$ cells to mesenchymal lineages, strongly indicate that the clonogenic *Ebf2*$^+$ cells represent MSCs.

Another important finding in the present study is the enrichment of CFU-Fs in *Ebf2*$^+$ cells, as indicated by the fact that one in six *Ebf2*$^+$ cells is under hypoxic conditions. The CFU-F frequency of the *Ebf2*$^+$ cells was comparable to that in the previously defined PαS cells (11) and was higher than that in *Nestin*$^+$ cells (10). This finding, together with the observation that the majority of the *Ebf2*$^+$ cells express SCA1, PDGFRα, and nestin, as revealed by our phenotypic and molecular analyses, suggested that the *Ebf2*$^+$ cells partly overlap with PαS and *Nestin*$^+$ cells. The CFU-F frequency of the PαS is higher in our study than that reported previously, likely due to the fact that the sorted cells in our study were cultured in hypoxic conditions, allowing for better growth of MSCs (44). Although CFU-Fs could also be detected outside the *Ebf2*$^-$ compartment when the cells were plated at a high density (>1,000 cells/cm^2), the cloning frequency of the *Ebf2*$^-$ cells was several hundredfold lower than that in *Ebf2*$^+$ cells.

The self-renewal property of the *Ebf2*$^+$ cells was suggested by the maintenance of CFU-F activity of a single *Ebf2*$^+$ cell clone during *in vivo* transplantation and *in vitro* serial replating assays. The donor-derived cells contain CFU-Fs with retained capacity to differentiate into multiple lineages after transplantation. The progeny of *Ebf2*$^+$ cells retained clonogenic capacities and molecular properties similar to those of their parental cells. The sustainable expansion of *Ebf2*$^+$ cells *in vitro* and the ability to generate *Ebf2*$^-$ progeny *in vivo* suggested a possible developmental hierarchy where *Ebf2* expression is associated with the stem cell properties of stromal cells.

In agreement with recent findings on natural phenotype of MSCs (11, 12, 14, 37, 40), the *Ebf2*$^+$ cells lack CD44 expression but highly express PDGFRα, CD90, CD29, CD34, CD105, and SCA1. The expression of SCA1 on the majority of the *Ebf2*-expressing cells from BM would argue against that any major fraction of the cells represents osteoblast-restricted progenitors reported to be SCA1$^-$ (40). In keeping with this finding, mRNA encoding a set of MSC-associated cell surface markers, including *Thy1/CD90*, *Ly6a/Sca1*, *Cd34*, *Pdgfra*, and *Cd51/Integrin αV*, are highly expressed in the *Ebf2*$^+$ cells, the combination of which may be used to replace the intracellular marker *Ebf2* for the prospective isolation of purified primary MSCs. Further enrichment of CFU-Fs in SCA1$^+$ *Ebf2*$^+$ cells compared to SCA1$^+$ *Ebf2*$^-$ cell subsets suggests heterogeneity of the *Ebf2*$^+$ cells.

Our global gene expression analysis on freshly isolated *Ebf2*-expressing cells provides new insight into the biological activities of MSCs since previous microarray analysis has been done on cultured cells (16, 46) or the cells with low CFU-F frequency (10). Consistent with the quiescent state of the *Ebf2*$^+$ cells, revealed by the KI67 analysis by FACS, the cell cycle inhibitor genes were upregulated, and the cell cycle progression genes were downregulated in *Ebf2*$^+$ cells. We also noted high levels of gene expression of growth factors including *Nov*, *Angiopoietin-like 1*, and *Igf1*, a direct target for *Ebf2* (48), and extracellular matrix proteins such as collagens, laminins, necdin, fibromodulin, decorin, and fibronectin. This finding makes the *Ebf2*$^+$ cells potentially interesting for the future study of regulation of early hematopoiesis, since several of those molecules have been shown to be important for hematopoietic stem cell expansion (49–52) and migration (25, 53). The *Ebf*-deficient mice display a male infertility (54), mild bone deformities and hematopoiesis defects (15, 16). The rather modest defects could be explained by that the *Ebf2*$^+$ cells express other *Ebf* family members that may functionally compensate for a loss of *Ebf2* within the mesenchymal compartment (55).

In summary, we have provided evidence that the *Ebf2*-expressing cells are not osteoblast lineage-restricted progenitor cells but rather represent an MSC population with self-renewal potential and multipotency in adult mouse BM. Molecular profile and functional properties of the *Ebf2*-expressing cells provide new insights into the natural activity of an MSC population. This finding opens new possibilities to investigate both the developmental hierarchy of mesenchymal cells and the cellular communication between hematopoietic cells and their microenvironmental cells of the BM in health and disease.

ACKNOWLEDGMENTS

We thank Liselotte Lenner in Linköping University in Sweden and Marta Florio San Raffaele Scientific Institute, Milan, Italy, for valuable advice and technical assistance.

This study was supported by the postdoctoral fellowship from the Swedish Research Council (K2008-77PK-20879-01-2) and the Cancerfonden (CAN 2009/1589). This study was also supported by running grants from the Swedish Research Council (2009-2675), the Cancerfonden (CAN 2012-2015), AFA Insurance Regenerative Medicine Program, and the Faculty of Medicine at Linköping University.

H.Q. designed research, performed research, collected data, analyzed and interpreted data, performed statistical analysis, and wrote the manuscript. M.S. designed research, analyzed and interpreted data, and wrote the manuscript. N.P. contributed to the differentiation experiments, and K.N. contributed to the histology. J.S. established the *Ebf2* reporter transgenic mouse breeding. F.C., A.B., and G.G.C. designed, generated, and validated the *Ebf2-CreER^{T2}* transgenic line.

REFERENCES

1. **Arai F, Hirao A, Ohmura M, Sato H, Matsuoka S, Takubo K, Ito K, Koh GY, Suda T.** 2004. Tie2/angiopoietin-1 signaling regulates hematopoietic stem cell quiescence in the bone marrow niche. Cell **118**:149–161.
2. **Calvi LM, Adams GB, Weibrecht KW, Weber JM, Olson DP, Knight MC, Martin RP, Schipani E, Divieti P, Bringhurst FR, Milner LA, Kronenberg HM, Scadden DT.** 2003. Osteoblastic cells regulate the haematopoietic stem cell niche. Nature **425**:841–846.
3. **Kiel MJ, Yilmaz OH, Iwashita T, Terhorst C, Morrison SJ.** 2005. SLAM family receptors distinguish hematopoietic stem and progenitor cells and reveal endothelial niches for stem cells. Cell **121**:1109–1121.
4. **Shiozawa Y, Havens AM, Pienta KJ, Taichman RS.** 2008. The bone marrow niche: habitat to hematopoietic and mesenchymal stem cells, and unwitting host to molecular parasites. Leukemia **22**:941–950.
5. **Friedenstein AJ, Chailakhyan RK, Latsinik NV, Panasyuk AF, Keiliss-Borok IV.** 1974. Stromal cells responsible for transferring the microenvironment of the hemopoietic tissues: cloning in vitro and retransplantation in vivo. Transplantation **17**:331–340.

6. **Pittenger MF, Mackay AM, Beck SC, Jaiswal RK, Douglas R, Mosca JD, Moorman MA, Simonetti DW, Craig S, Marshak DR.** 1999. Multilineage potential of adult human mesenchymal stem cells. Science **284**:143–147.
7. **Valtieri M, Sorrentino A.** 2008. The mesenchymal stromal cell contribution to homeostasis. J. Cell Physiol. **217**:296–300.
8. **Anjos-Afonso F, Bonnet D.** 2007. Nonhematopoietic/endothelial SSEA-1^{+} cells define the most primitive progenitors in the adult murine bone marrow mesenchymal compartment. Blood **109**:1298–1306.
9. **Sarugaser R, Hanoun L, Keating A, Stanford WL, Davies JE.** 2009. Human mesenchymal stem cells self-renew and differentiate according to a deterministic hierarchy. PLoS One **4**:e6498. doi:10.1371/journal.pone.0006498.
10. **Mendez-Ferrer S, Michurina TV, Ferraro F, Mazloom AR, Macarthur BD, Lira SA, Scadden DT, Ma'ayan A, Enikolopov GN, Frenette PS.** 2010. Mesenchymal and haematopoietic stem cells form a unique bone marrow niche. Nature **466**:829–834.
11. **Morikawa S, Mabuchi Y, Kubota Y, Nagai Y, Niibe K, Hiratsu E, Suzuki S, Miyauchi-Hara C, Nagoshi N, Sunabori T, Shimmura S, Miyawaki A, Nakagawa T, Suda T, Okano H, Matsuzaki Y.** 2009. Prospective identification, isolation, and systemic transplantation of multipotent mesenchymal stem cells in murine bone marrow. J. Exp. Med. **206**:2483–2496.
12. **Peister A, Mellad JA, Larson BL, Hall BM, Gibson LF, Prockop DJ.** 2004. Adult stem cells from bone marrow (MSCs) isolated from different strains of inbred mice vary in surface epitopes, rates of proliferation, and differentiation potential. Blood **103**:1662–1668.
13. **Short BJ, Brouard N, Simmons PJ.** 2009. Prospective isolation of mesenchymal stem cells from mouse compact bone. Methods Mol. Biol. **482**:259–268.
14. **Qian H, Le Blanc K, Sigvardsson M.** 2012. Primary mesenchymal stem and progenitor cells from bone marrow lack expression of CD44 protein. J. Biol. Chem. **287**:25795–25807.
15. **Kieslinger M, Folberth S, Dobreva G, Dorn T, Croci L, Erben R, Consalez GG, Grosschedl R.** 2005. EBF2 regulates osteoblast-dependent differentiation of osteoclasts. Dev. Cell **9**:757–767.
16. **Kieslinger M, Hiechinger S, Dobreva G, Consalez GG, Grosschedl R.** 2010. Early B cell factor 2 regulates hematopoietic stem cell homeostasis in a cell-nonautonomous manner. Cell Stem Cell **7**:496–507.
17. **Akerblad P, Lind U, Liberg D, Bamberg K, Sigvardsson M.** 2002. Early B-cell factor (O/E-1) is a promoter of adipogenesis and involved in control of genes important for terminal adipocyte differentiation. Mol. Cell. Biol. **22**:8015–8025.
18. **Hagman J, Gutch MJ, Lin H, Grosschedl R.** 1995. EBF contains a novel zinc coordination motif and multiple dimerization and transcriptional activation domains. EMBO J. **14**:2907–2916.
19. **Garel S, Marin F, Mattei MG, Vesque C, Vincent A, Charnay P.** 1997. Family of Ebf/Olf-1-related genes potentially involved in neuronal differentiation and regional specification in the central nervous system. Dev. Dynamics **210**:191–205.
20. **Wang SS, Lewcock JW, Feinstein P, Mombaerts P, Reed RR.** 2004. Genetic disruptions of O/E2 and O/E3 genes reveal involvement in olfactory receptor neuron projection. Development **131**:1377–1388.
21. **Lagergren A, Mansson R, Zetterblad J, Smith E, Basta B, Bryder D, Akerblad P, Sigvardsson M.** 2007. The Cxcl12, periostin, and Ccl9 genes are direct targets for early B-cell factor in OP-9 stroma cells. J. Biol. Chem. **282**:14454–14462.
22. **Gong S, Zheng C, Doughty ML, Losos K, Didkovsky N, Schambra UB, Nowak NJ, Joyner A, Leblanc G, Hatten ME, Heintz N.** 2003. A gene expression atlas of the central nervous system based on bacterial artificial chromosomes. Nature **425**:917–925.
23. **Copeland NG, Jenkins NA, Court DL.** 2001. Recombineering: a powerful new tool for mouse functional genomics. Nat. Rev. Genet. **2**:769–779.
24. **Warming S, Costantino N, Court DL, Jenkins NA, Copeland NG.** 2005. Simple and highly efficient BAC recombineering using *galK* selection. Nucleic Acids Res. **33**:e36.
25. **Qian H, Tryggvason K, Jacobsen SE, Ekblom M.** 2006. Contribution of alpha6 integrins to hematopoietic stem and progenitor cell homing to bone marrow and collaboration with alpha4 integrins. Blood **107**:3503–3510.
26. **Hu M, Krause D, Greaves M, Sharkis S, Dexter M, Heyworth C, Enver T.** 1997. Multilineage gene expression precedes commitment in the hemopoietic system. Genes Dev. **11**:774–785.
27. **Mansson R, Hultquist A, Luc S, Yang L, Anderson K, Kharazi S, Al-Hashmi S, Liuba K, Thoren L, Adolfsson J, Buza-Vidas N, Qian H, Soneji S, Enver T, Sigvardsson M, Jacobsen SE.** 2007. Molecular evidence for hierarchical transcriptional lineage priming in fetal and adult stem cells and multipotent progenitors. Immunity **26**:407–419.
28. **Wang Y, Sul HS.** 2009. Pref-1 regulates mesenchymal cell commitment and differentiation through Sox9. Cell Metab. **9**:287–302.
29. **Nygren JM, Jovinge S, Breitbach M, Sawen P, Roll W, Hescheler J, Taneera J, Fleischmann BK, Jacobsen SE.** 2004. Bone marrow-derived hematopoietic cells generate cardiomyocytes at a low frequency through cell fusion, but not transdifferentiation. Nat. Med. **10**:494–501.
30. **Zetterblad J, Qian H, Zandi S, Mansson R, Lagergren A, Hansson F, Bryder D, Paulsson N, Sigvardsson M.** 2010. Genomics based analysis of interactions between developing B-lymphocytes and stromal cells reveal complex interactions and two-way communication. BMC Genomics **11**:108. doi:10.1186/1471-2164-11-108.
31. **Abdallah BM, Ditzel N, Kassem M.** 2008. Assessment of bone formation capacity using *in vivo* transplantation assays: procedure and tissue analysis. Methods Mol. Biol. **455**:89–100.
32. **Srinivas S, Watanabe T, Lin CS, William CM, Tanabe Y, Jessell TM, Costantini F.** 2001. Cre reporter strains produced by targeted insertion of EYFP and ECFP into the *ROSA26* locus. BMC Dev. Biol. **1**:4. doi:10.1186/1471-213X-1-4.
33. **Williams B, Nilsson SK.** 2009. Investigating the interactions between haemopoietic stem cells and their niche: methods for the analysis of stem cell homing and distribution within the marrow following transplantation. Methods Mol. Biol. **482**:93–107.
34. **Hooper AT, Butler JM, Nolan DJ, Kranz A, Iida K, Kobayashi M, Kopp HG, Shido K, Petit I, Yanger K, James D, Witte L, Zhu Z, Wu Y, Pytowski B, Rosenwaks Z, Mittal V, Sato TN, Rafii S.** 2009. Engraftment and reconstitution of hematopoiesis is dependent on VEGFR2-mediated regeneration of sinusoidal endothelial cells. Cell Stem Cell **4**:263–274.
35. **Chamberlain G, Fox J, Ashton B, Middleton J.** 2007. Concise review: mesenchymal stem cells: their phenotype, differentiation capacity, immunological features, and potential for homing. Stem Cells **25**:2739–2749.
36. **Delorme B, Ringe J, Gallay N, Le Vern Y, Kerboeuf D, Jorgensen C, Rosset P, Sensebe L, Layrolle P, Haupl T, Charbord P.** 2008. Specific plasma membrane protein phenotype of culture-amplified and native human bone marrow mesenchymal stem cells. Blood **111**:2631–2635.
37. **Eslaminejad MB, Nadri S, Hosseini RH.** 2007. Expression of Thy 1.2 surface antigen increases significantly during the murine mesenchymal stem cells cultivation period. Dev. Growth Differ. **49**:351–364.
38. **Lee RH, Seo MJ, Pulin AA, Gregory CA, Ylostalo J, Prockop DJ.** 2009. The CD34-like protein PODXL and alpha6-integrin (CD49f) identify early progenitor MSCs with increased clonogenicity and migration to infarcted heart in mice. Blood **113**:816–826.
39. **Sun S, Guo Z, Xiao X, Liu B, Liu X, Tang PH, Mao N.** 2003. Isolation of mouse marrow mesenchymal progenitors by a novel and reliable method. Stem Cells **21**:527–535.
40. **Nakamura Y, Arai F, Iwasaki H, Hosokawa K, Kobayashi I, Gomei Y, Matsumoto Y, Yoshihara H, Suda T.** 2010. Isolation and characterization of endosteal niche cell populations that regulate hematopoietic stem cells. Blood **116**:1422–1432.
41. **Cheng T, Rodrigues N, Shen H, Yang Y, Dombkowski D, Sykes M, Scadden DT.** 2000. Hematopoietic stem cell quiescence maintained by p21$^{cip1/waf1}$. Science **287**:1804–1808.
42. **Qian H, Buza-Vidas N, Hyland CD, Jensen CT, Antonchuk J, Mansson R, Thoren LA, Ekblom M, Alexander WS, Jacobsen SE.** 2007. Critical role of thrombopoietin in maintaining adult quiescent hematopoietic stem cells. Cell Stem Cell **1**:671–684.
43. **Yoshihara H, Arai F, Hosokawa K, Hagiwara T, Takubo K, Nakamura Y, Gomei Y, Iwasaki H, Matsuoka S, Miyamoto K, Miyazaki H, Takahashi T, Suda T.** 2007. Thrombopoietin/MPL signaling regulates hematopoietic stem cell quiescence and interaction with the osteoblastic niche. Cell Stem Cell **1**:685–697.
44. **Tsai CC, Chen YJ, Yew TL, Chen LL, Wang JY, Chiu CH, Hung SC.** 2011. Hypoxia inhibits senescence and maintains mesenchymal stem cell properties through down-regulation of E2A-p21 by HIF-TWIST. Blood **117**:459–469.
45. **Delorme B, Ringe J, Pontikoglou C, Gaillard J, Langonne A, Sensebe L, Noel D, Jorgensen C, Haupl T, Charbord P.** 2009. Specific lineage-priming of bone marrow mesenchymal stem cells provides the molecular framework for their plasticity. Stem Cells **27**:1142–1151.
46. **Tanabe S, Sato Y, Suzuki T, Suzuki K, Nagao T, Yamaguchi T.** 2008.

Gene expression profiling of human mesenchymal stem cells for identification of novel markers in early- and late-stage cell culture. J. Biochem. **144**:399–408.
47. **Tormin A, Brune JC, Olsson E, Valcich J, Neuman U, Olofsson T, Jacobsen SE, Scheding S.** 2009. Characterization of bone marrow-derived mesenchymal stromal cells (MSC) based on gene expression profiling of functionally defined MSC subsets. Cytotherapy **11**:114–128.
48. **Croci L, Barili V, Chia D, Massimino L, van Vugt R, Masserdotti G, Longhi R, Rotwein P, Consalez GG.** 2011. Local insulin-like growth factor I expression is essential for Purkinje neuron survival at birth. Cell Death Differ. **18**:48–59.
49. **Gupta R, Hong D, Iborra F, Sarno S, Enver T.** 2007. NOV (CCN3) functions as a regulator of human hematopoietic stem or progenitor cells. Science **316**:590–593.
50. **Mayack SR, Shadrach JL, Kim FS, Wagers AJ.** 2010. Systemic signals regulate ageing and rejuvenation of blood stem cell niches. Nature **463**:495–500.
51. **Panzenbock B, Bartunek P, Mapara MY, Zenke M.** 1998. Growth and differentiation of human stem cell factor/erythropoietin-dependent erythroid progenitor cells in vitro. Blood **92**:3658–3668.
52. **Zhang CC, Kaba M, Ge G, Xie K, Tong W, Hug C, Lodish HF.** 2006. Angiopoietin-like proteins stimulate ex vivo expansion of hematopoietic stem cells. Nat. Med. **12**:240–245.
53. **Mendez-Ferrer S, Frenette PS.** 2007. Hematopoietic stem cell trafficking: regulated adhesion and attraction to bone marrow microenvironment. Ann. N. Y. Acad. Sci. **1116**:392–413.
54. **Corradi A, Croci L, Broccoli V, Zecchini S, Previtali S, Wurst W, Amadio S, Maggi R, Quattrini A, Consalez GG.** 2003. Hypogonadotropic hypogonadism and peripheral neuropathy in Ebf2-null mice. Development **130**:401–410.
55. **Jimenez MA, Akerblad P, Sigvardsson M, Rosen ED.** 2007. Critical role for Ebf1 and Ebf2 in the adipogenic transcriptional cascade. Mol. Cell. Biol. **27**:743–757.